# 8

# The Structure of the Nucleon

Elastic and deep inelastic scattering from nucleons, 1956–1973.

Hadronic scattering experiments produced extensive and rich data revealing resonances and regularities of cross sections. While the quark model provided a firm basis for classifying the particles and resonances, the scattering cross sections were less easily interpreted. The early studies of strong interactions indicated that the couplings of the particles were large. This precluded the straightforward use of perturbation theory. While alternative approaches have yielded some important results, it is still true that even processes as basic as elastic proton–proton scattering are beyond our ability to explain in detail. In contradistinction, scattering of electrons by protons and neutrons is open to direct interpretation.

For the scattering of an electron by a proton it is a good approximation to assume that the interaction is due to the exchange of a single virtual photon. The small corrections to this approximation may be calculated if necessary. Each coupling of the photon gives a factor of $e$ in the scattering amplitude, so a virtual photon's two couplings typically provides a factor $\alpha = e^2/4\pi \approx 1/137$. It is this small number that makes the approximation a good one.

The scattering of relativistic electrons ($E >> m_e$) by a known charge distribution can be calculated using the standard methods of quantum mechanics. If the electron were spinless and scattered from a static point charge, the cross section would be given by the Rutherford formula:

$$\frac{d\sigma}{d\Omega} = \frac{\alpha^2}{4E^2 \sin^4 \frac{1}{2}\theta}, \tag{8.1}$$

where $E$ is the energy of the incident relativistic electron and $\theta$ is its scattering angle in the laboratory. Taking into account the electron's spin gives the Mott cross section:

$$\frac{d\sigma}{d\Omega} = \frac{\alpha^2 \cos^2 \frac{1}{2}\theta}{4E^2 \sin^4 \frac{1}{2}\theta}. \tag{8.2}$$



Downloaded from https://www.cambridge.org/core. UNIVERSIDAD AUTONOMA METROPOLITANA, on 17 Nov 2026 at 09:09:05, subject to the Cambridge Core terms of use, available at https://www.cambridge.org/core/terms. https://doi.org/10.1017/9780511609923.010

If the electron is scattered by a static source, its final energy, $E'$, is the same as the incident energy $E$, and the four-momentum transfer squared is $q^2 = -4E^2 \sin^2 \frac{1}{2}\theta$. If the target has finite mass, $M$, and thus recoils, then for elastic scattering

$$E' = \frac{E}{1 + \frac{2E}{M} \sin^2 \frac{1}{2}\theta}, \tag{8.3}$$

$$q^2 = -4EE' \sin^2 \tfrac{1}{2}\theta. \tag{8.4}$$

The elastic scattering of an electron by a pointlike Dirac particle of mass $M$ has a cross section

$$\frac{d\sigma}{d\Omega} = \frac{\alpha^2 \cos^2 \frac{1}{2}\theta}{4E^2 \sin^4 \frac{1}{2}\theta} \cdot \frac{E'}{E} \left[ 1 - \frac{q^2}{2M^2} \tan^2 \tfrac{1}{2}\theta \right], \tag{8.5}$$

which reduces to the Mott cross section as the target mass increases.

These simple results do not apply if the charge distribution of the target has some spatial extent. In the case of elastic scattering from a fixed charge distribution, $\rho(r)$, the scattering amplitude is modified by a form factor

$$F(q^2) = \int d^3r e^{i\mathbf{q}\cdot\mathbf{r}} \rho(r), \tag{8.6}$$

so the Rutherford or Mott cross section would be multiplied by the factor $|F(q^2)|^2$. Since $\int d^3r \rho(r) = 1$, the form factor reduces to unity for zero momentum transfer.

A relativistic treatment of the scattering of electrons by protons is obtained by writing the scattering amplitude as a product of three factors:

$$\mathcal{M} = \frac{4\pi\alpha}{q^2} J_\mu^{electron}(q) J^{\mu\ proton}(q), \tag{8.7}$$

where $q$ is the four-momentum exchanged between the electron and the proton. The factor $1/q^2$ arises from the exchange of the virtual photon between the two. The current due to the electron is

$$J_\mu^{electron} = \overline{u}(k_\mathrm{f}) \gamma_\mu u(k_\mathrm{i}) \tag{8.8}$$

where $k_\mathrm{i}$ and $k_\mathrm{f}$ are the initial and final electron momenta and $\overline{u}$ and $u$ are Dirac spinors as described in Chapter 6. The electromagnetic current for the proton involves two form factors,

$$J_\mu^{proton} = \overline{u}(p_\mathrm{f}) \left[ F_1(q^2) \gamma_\mu + i \frac{q^\nu \sigma_{\mu\nu} \kappa}{2M} F_2(q^2) \right] u(p_\mathrm{i}). \tag{8.9}$$

Here $p_\mathrm{i}$ and $p_\mathrm{f}$ are the initial and final proton momenta and $q = k_\mathrm{i} - k_\mathrm{f} = p_\mathrm{f} - p_\mathrm{i}$ is the four-momentum transfer. The second term, proportional to the form factor $F_2(q^2)$, is the

Downloaded from https://www.cambridge.org/core. UNIVERSIDAD AUTONOMA METROPOLITANA, on 17 Nov 2026 at 09:09:05, subject to the Cambridge Core terms of use, available at https://www.cambridge.org/core/terms. https://doi.org/10.1017/9780511609923.010

anomalous magnetic moment coupling and $\kappa = 1.79$ is the anomalous magnetic moment of the proton in units of the nuclear magneton, $e\hbar/(2Mc)$. The form factors, $F_1(q^2)$ and $F_2(q^2)$, are the analogs of $F(q^2)$ in the discussion above, and $F_1(0) = F_2(0) = 1$. If the proton were a pointlike Dirac particle like the electron, we would have instead $F_1(q^2) = 1$ and $\kappa F_2(q^2) = 0$. For a neutron, since the total charge is zero, $F_1(0) = 0$. The value of $\kappa$ for the neutron is $-1.91$.

From these currents the differential cross section for elastic electron–proton scattering can be calculated in terms of the form factors. The result is known as the Rosenbluth formula:

$$\frac{d\sigma}{d\Omega} = \frac{\alpha^2 \cos^2 \tfrac{1}{2}\theta}{4E^2 \sin^4 \tfrac{1}{2}\theta} \cdot \frac{E'}{E} \cdot \left[ \left( F_1^2 + \frac{\kappa^2 Q^2}{4M^2} F_2^2 \right) + \frac{Q^2}{2M^2} (F_1 + \kappa F_2)^2 \tan^2 \tfrac{1}{2}\theta \right], \quad (8.10)$$

where $\theta$ is the scattering angle of the electron in the laboratory and $E$ is its initial energy. We have written $Q^2$ for $-q^2$, so $Q^2$ is positive.

The Rosenbluth formula follows from the assumption that a single photon is exchanged between the electron and the proton. All of our ignorance is subsumed in the two form factors, $F_1(Q^2)$ and $F_2(Q^2)$. The formula can be tested by multiplying the observed cross section by $(E^3/E')\sin^2\tfrac{1}{2}\theta \tan^2\tfrac{1}{2}\theta$ and plotting the result at fixed $Q^2$ as a function of $\tan^2\tfrac{1}{2}\theta$. The result should be a straight line.

Elastic electron–proton scattering was measured by McAllister and Hofstadter using 188-MeV electrons **(Ref. 8.1)** produced by a linear accelerator at Stanford. The electrons scattered from a hydrogen target into a spectrometer that could be rotated around the interaction region.

The experiment was able to determine the root-mean-square charge radius of the proton by measuring the form factors at low momentum transfer. In this region, we can expand

$$\begin{aligned} F(q^2) &= \int d^3r \rho(r) \exp(i\mathbf{q}\cdot\mathbf{r}) \\ &= \int d^3r \rho(r)[1 + i\mathbf{q}\cdot\mathbf{r} - (1/2)(\mathbf{q}\cdot\mathbf{r})^2 \cdots] \\ &= 1 - \frac{\mathbf{q}^2}{6} < r^2 > \cdots \end{aligned} \quad (8.11)$$

Assuming the same $< r^2 >$ applied to both form factors, McAllister and Hofstadter found $< r^2 >^{1/2} = 0.74 \pm 0.24$ fm.

Form factors exist as well for excitation processes like $ep \rightarrow e\Delta(1232)$. The number of form factors depends on the initial and final spins. The form factors are expected generally to decrease with momentum transfer, reflecting the spread in the charge and current distributions of the initial and final particles.

In the late 1960s, under the leadership of "Pief" Panofsky, the Stanford Linear Accelerator Center, SLAC, opened a vast new energy domain for exploration. The two-mile long accelerator produced electrons with energies up to about 18 GeV. The scattered electrons were detected and measured by very large magnetic spectrometers. At these high energies,

Downloaded from https://www.cambridge.org/core. UNIVERSIDAD AUTONOMA METROPOLITANA, on 17 Nov 2026 at 09:09:05, subject to the Cambridge Core terms of use, available at https://www.cambridge.org/core/terms. https://doi.org/10.1017/9780511609923.010

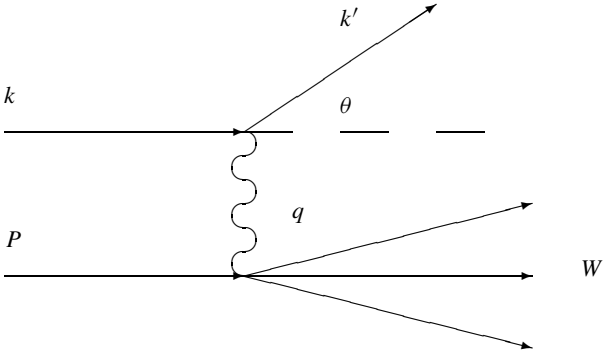



Figure 8.1. The kinematics of deep inelastic lepton–nucleon scattering. The incident lepton and proton have four-momenta $k$ and $P$, respectively. The scattered lepton has four-momentum $k' = k - q$. The mass squared of the produced hadronic system is $W^2 = (P + q)^2$. The fundamental variables are $Q^2 = -q^2 = 4EE' \sin^2 \frac{1}{2}\theta$ and $\nu = E - E'$, where $E$ and $E'$ are the initial and final lepton energies in the lab, and $\theta$ is the lab scattering angle of the lepton. The mass of the nucleon is $M$ so $q \cdot P = (k - k') \cdot P = M\nu$, and $W^2 = M^2 + 2M\nu - Q^2$.

much of the scattering was inelastic, typically $ep \to ep\pi\pi...$ or $ep \to en\pi\pi...$. When the scattering is not elastic, the energy and direction of the scattered electron are independent variables, unlike the elastic scattering situation. From careful measurements of the direction, specified by a solid angle element $d\Omega$, and the energy $E'$ of the scattered electron, the four-momentum transfer can be calculated. In this way, the differential cross section, $d\sigma/d\Omega dE'$ is determined as a function of $E'$ and $Q^2$. The outgoing hadrons were generally not detected. The kinematics are shown in Figure 8.1.

A SLAC–MIT group (**Ref. 8.2**) scattered electrons from a hydrogen target and detected the outgoing electrons in a large magnetic spectrometer set at angles $\theta = 6^\circ$ and $10^\circ$. The scattered electrons' momenta were measured to 0.1%, and the spectrometer accepted a momentum interval $\Delta p/p = 3.5\%$. The potential background produced by charged pions entering the spectrometers was suppressed by observing the electron showers.

As expected, the data showed peaks when the mass $W$ of the produced hadronic system corresponded to the mass of one of the resonances in the sequence $N^*$ ($I = 1/2$ nonstrange baryons) or $\Delta$ ($I = 3/2$ nonstrange baryons). Each resonance showed the expected behavior as a function of $Q^2$. The production fell with increasing momentum transfer. What was surprising was that for $W$ values beyond the resonances, the cross section did not fall with increasing $Q^2$.

Just as it is possible to write down a most general expression for the electromagnetic current of a proton for elastic scattering, it is possible to write down a general expression for the differential cross section measured in inelastic electron scattering when only the electron is measured in the final state. This expression depends on two functions, $W_1$ and $W_2$. These *structure functions* depend on two variables, $\nu$, the energy lost by the electron

Downloaded from https://www.cambridge.org/core. UNIVERSIDAD AUTONOMA METROPOLITANA, on 17 Nov 2026 at 09:09:05, subject to the Cambridge Core terms of use, available at https://www.cambridge.org/core/terms. https://doi.org/10.1017/9780511609923.010

in the laboratory, and $Q^2$. The full expression for the differential cross section is

$$\frac{d\sigma}{d\Omega dE'} = \frac{\alpha^2}{4E^2}\frac{\cos^2\frac{1}{2}\theta}{\sin^4\frac{1}{2}\theta}\left[W_2 + 2W_1\tan^2\tfrac{1}{2}\theta\right]. \tag{8.12}$$

This expression contains the Mott cross section as a factor and is analogous to the Rosenbluth formula. It follows from the assumption of single photon exchange and isolates the unknown physics in two functions, $W_1$ and $W_2$. Here, however, these are functions of two variables, $\nu$ and $Q^2$, not just one. In contrast, for elastic scattering, $(P+q)^2 = M^2$ so the two variables are not independent but rather are related by $Q^2 = 2M\nu$.

To determine $W_1$ and $W_2$ separately it is necessary to measure the differential cross section at two values of $E'$ and $\theta$ that correspond to the same values of $\nu$ and $Q^2$. This is possible by varying the incident energy, $E$. At small values of $\theta$, $W_2$ dominates, so it is most convenient to focus on this quantity.

The most important result of the experiment at SLAC was the discovery that $\nu W_2$ did not fall with increasing $Q^2$, but instead tended to a value that depended on the single variable $\omega = 2M\nu/Q^2$ **(Ref. 8.3)**. This behavior, termed "scaling," had been anticipated first by Bjorken on the basis of a very complex study. By 1967, Bjorken was examining deep inelastic scattering by imagining the nucleon to be composed of pointlike quarks.

In an independent effort, Feynman had concluded from his analysis of hadronic collisions, that the proton ought to be composed of pointlike constituents, "partons" he called them. They shared the total momentum of the proton by taking up variable fractions, $x$, of that momentum. The probability of a parton carrying a fraction between $x$ and $x + dx$ was written $f(x)dx$. The essential feature was that the function $f(x)$ was not to depend on the process at hand nor the energy of the proton, but was intrinsic to the proton so long as the proton had a large momentum. It was natural to assume that the partons were, in fact, quarks. There would not be just three quarks in a proton because in addition there could be many quark–antiquark pairs. The distribution functions for the various quarks were indicated by $u(x)$, $d(x)$, $\overline{u}(x)$, etc. Since the momenta had to add up to the proton's momentum, there was a constraint

$$\int dx\, x[u(x) + \overline{u}(x) + d(x) + \overline{d}(x) + ...] = 1. \tag{8.13}$$

As we shall see later, there is also a contribution from the uncharged constituents in the nucleon. In order for the quantum numbers of the proton to come out correctly, other conditions had to be satisfied:

$$\begin{aligned}\int dx[u(x) - \overline{u}(x)] &= 2,\\ \int dx[d(x) - \overline{d}(x)] &= 1,\\ \int dx[s(x) - \overline{s}(x)] &= 0.\end{aligned} \tag{8.14}$$

Downloaded from https://www.cambridge.org/core. UNIVERSIDAD AUTONOMA METROPOLITANA, on 17 Nov 2026 at 09:09:05, subject to the Cambridge Core terms of use, available at https://www.cambridge.org/core/terms. https://doi.org/10.1017/9780511609923.010

These replaced the statement that the proton was composed of two $u$ quarks and a $d$ quark. Thus in Feynman's model these "valence" quarks were supplemented by a "sea" of quark–antiquark pairs.

The combination of Bjorken's and Feynman's studies was a perfect explanation of "scaling," *i.e.* the dependence of $\nu W_2$ on the quantity $\omega$ alone. If the quark-partons were treated as real particles that had to be on-shell (that is, satisfied the relation $p^2 = E^2 - \mathbf{p}^2 = m^2$) both before and after being scattered by the virtual photon, then $p_f^2 = (p_i + q)^2 = (xP + q)^2 \approx 0$ if the masses of the quarks and the proton could be ignored, as seemed reasonable for very high energy collisions. From this followed

$$Q^2 = 2xP \cdot q = 2xM\nu. \tag{8.15}$$

This meant that the fraction $x$ of the proton's momentum carried by the struck quark was simply the reciprocal of $\omega$, the variable singled out in the experiment at SLAC. If the probability of there being a quark with momentum fraction $x$ did not depend on the details of the event, scaling would follow, provided the scattering could be viewed as the incoherent sum of the scattering by the individual partons.

The precise connection between the parton distributions and the structure functions can be obtained by expressing the cross sections in terms of the Lorentz invariant variables $s = 2ME$, $x = Q^2/2M\nu$ and $y = \nu/E$. It is traditional to write $MW_1 = F_1$ and $\nu W_2 = F_2$. The dimensionless function $F_1$ and $F_2$, which must not be confused with the form factors of elastic scattering, are thus nominally functions of both $x$ and $Q^2$. Substitution into the formula defining $W_1$ and $W_2$ gives

$$\frac{d\sigma}{dx\,dy} = \frac{4\pi\alpha^2 s}{Q^4}\left\{\frac{1}{2}[1 + (1-y)^2]\,2xF_1 + (1-y)(F_2 - 2xF_1) - \frac{M}{2E}xyF_2\right\}. \tag{8.16}$$

This can be compared with the cross section for the scattering of an electron by a pointlike Dirac particle of unit charge carrying a fraction $x$ of the proton's momentum. The cross section, which can be derived from the cross section given above for an electron on a pointlike Dirac particle, is

$$\frac{d\sigma}{dy} = \frac{4\pi\alpha^2 xs}{Q^4}\left\{\frac{1}{2}[1 + (1-y)^2] - \frac{M}{2E}xy\right\}. \tag{8.17}$$

By comparing the results, we deduce the values of $F_1$ and $F_2$:

$$F_1 \equiv MW_1 = \frac{1}{2}\left[\frac{4}{9}u(x) + \frac{1}{9}d(x) + \frac{4}{9}\overline{u}(x) + \frac{1}{9}\overline{d}(x) + \cdots\right], \tag{8.18}$$

$$F_2 \equiv \nu W_2 = x\left[\frac{4}{9}u(x) + \frac{1}{9}d(x) + \frac{4}{9}\overline{u}(x) + \frac{1}{9}\overline{d}(x) + \cdots\right], \tag{8.19}$$

where the factors 4/9 and 1/9 arise as the squares of the quark charges. The connection $F_2 = 2xF_1$, known as the Callan–Gross relation, is a consequence of taking the partons

Downloaded from https://www.cambridge.org/core. UNIVERSIDAD AUTONOMA METROPOLITANA, on 17 Nov 2026 at 09:09:05, subject to the Cambridge Core terms of use, available at https://www.cambridge.org/core/terms. https://doi.org/10.1017/9780511609923.010

to be pointlike Dirac particles. The absence of $Q^2$ dependence in $F_1$ and $F_2$ is the manifestation of scaling. With this stunningly simple formula, deep inelastic electron scattering becomes a powerful probe of the interior of the proton.

The simple parton picture was expected by Feynman to apply to very high energies. He reasoned that at high energies time dilation would cause the interactions between the partons to appear less frequent so that it would be a good approximation to ignore these interactions. Thus deep inelastic scattering could be regarded as the incoherent sum of the interactions with the individual partons.

A few years after these developments, important advances were made in understanding the theory of quantum chromodynamics (QCD). In this theory the interactions between quarks are the result of the exchange of vector particles called gluons. In many ways the theory is analogous to ordinary electrodynamics.

QCD finds very different behavior for quarks and gluons at short and long distances. Unlike the behavior of electric forces, the force between a quark and an antiquark does not decrease as their separation increases, but approaches a constant. Thus it takes an infinite amount of energy to separate them completely. Conversely, at short distances, the forces become weaker. It is the short-distance behavior that is probed in deep inelastic scattering, and thus QCD confirms Feynman's picture of non-interacting partons as the constituents of the proton.

Of course, the interactions between the quarks only decrease and do not disappear at short distances. As a result, the "kindergarten" parton model described above is only approximate. The quark and gluon distributions are weakly functions of $Q^2$ as well as $x$ and scaling is only approximately satisfied.

This phenomenon can be understood by analogy with bremsstrahlung as described in Chapter 2. When an electron scatters from an electromagnetic field, it emits photons and the greater the scattering, the more bremsstrahlung there is. When a quark scatters, it emits gluons and some of its momentum is given to the gluons. As the momentum transfer is increased, the fraction of its momentum lost to gluons increases. Thus a quark with momentum fraction $x$ at some low value of $Q^2$ becomes a quark with momentum fraction $x - x'$ and a gluon with momentum fraction $x'$ at some higher value of $Q^2$. Thus for large values of $x$, $u(x, Q^2)$ falls with increasing $Q^2$. For low values of $x$, $u(x, Q^2)$ may increase because quarks with higher $x$ may feed down quarks to it.

The parton model makes analogous predictions for deep inelastic neutrino scattering. Since the source of neutrino beams are the decays $\pi \rightarrow \mu\nu$ and $K \rightarrow \mu\nu$, $\nu_\mu$ greatly dominate over $\nu_e$ (see Chapter 6). Thus in deep inelastic neutrino scattering by nucleons, one observes

$$\nu_\mu + \text{nucleon} \rightarrow \mu^- + \text{hadrons}$$

and

$$\overline{\nu_\mu} + \text{nucleon} \rightarrow \mu^+ + \text{hadrons}.$$

Because parity is not conserved in weak interactions, there are more structure functions for neutrino scattering than for electron scattering. Three structure functions contribute in

Downloaded from https://www.cambridge.org/core. UNIVERSIDAD AUTONOMA METROPOLITANA, on 17 Nov 2026 at 09:09:05, subject to the Cambridge Core terms of use, available at https://www.cambridge.org/core/terms. https://doi.org/10.1017/9780511609923.010

the limit in which the lepton masses are ignored. If we use as variables $x = Q^2/2M\nu$ and $y = \nu/E$, the general forms are, in the context of the V-A theory,

$$\frac{d\sigma^{\nu}}{dx\,dy} = \frac{G_F^2 ME}{\pi}\left[(1-y)F_2^{\nu} + y^2 x F_1^{\nu} + (y - y^2/2)x F_3^{\nu}\right], \tag{8.20}$$

$$\frac{d\sigma^{\overline{\nu}}}{dx\,dy} = \frac{G_F^2 ME}{\pi}\left[(1-y)F_2^{\overline{\nu}} + y^2 x F_1^{\overline{\nu}} - (y - y^2/2)x F_3^{\overline{\nu}}\right]. \tag{8.21}$$

These forms are general (except that we have ignored the Cabibbo angle and corrections of order $M/E$) and $F_1^{\nu}$, $F_2^{\nu}$, and $F_3^{\nu}$ are functions of $Q^2$ and $\nu$. In the Bjorken limit ($\nu \to \infty$, $Q^2 \to \infty$, $2M\nu/Q^2 = x$ finite), the $F^{\nu}$'s are nearly functions of $x$ only.

The scattering of a neutrino by a pointlike fermion is much like the electromagnetic scattering of an electron by a pointlike fermion. In Chapter 6 we saw that the weak interaction current of the leptons has the V-A form, $\frac{1}{2}\gamma_\mu(1-\gamma_5)$. For massless fermions, the quantity $\frac{1}{2}(1-\gamma_5)$ projects out the left-handed piece of the fermion, while $\frac{1}{2}(1+\gamma_5)$ projects out the right-handed piece. Now the coupling of the electromagnetic field to the fermion is governed by the current

$$\overline{u}(p')\gamma_\mu u(p). \tag{8.22}$$

If we consider an incident left-handed fermion we can write

$$\overline{u}(p')\gamma_\mu \frac{1}{2}(1-\gamma_5)u(p) = \overline{u}(p')\frac{1}{2}(1+\gamma_5)\gamma_\mu u(p) \tag{8.23}$$

$$= \left[\frac{1}{2}(1-\gamma_5)u(p')\right]^{\dagger}\gamma_0\gamma_\mu u(p) \tag{8.24}$$

where, as usual the dagger indicates Hermitian conjugation. We see that the final fermion is also left-handed. Indeed, both vector and axial vector couplings have this property: the helicity (i.e. the projection of the spin along the direction of motion) of a massless fermion is unchanged by the interaction with an electromagnetic or weak current. It follows that we can consider the scattering as the incoherent sum of processes with specified helicities. We take as an example the electromagnetic process $e^-\mu^- \to e^-\mu^-$, ignoring the particle masses and using center-of-mass variables:

$$\frac{d\sigma}{d\Omega}(e_L^-\mu_L^- \to e_L^-\mu_L^-) = \frac{d\sigma}{d\Omega}(e_R^-\mu_R^- \to e_R^-\mu_R^-) = \frac{\alpha^2 s}{Q^4}, \tag{8.25}$$

$$\frac{d\sigma}{d\Omega}(e_L^-\mu_R^- \to e_L^-\mu_R^-) = \frac{d\sigma}{d\Omega}(e_R^-\mu_L^- \to e_R^-\mu_L^-) = \frac{\alpha^2 s}{Q^4}\frac{(1+\cos\theta)^2}{4}. \tag{8.26}$$

The presence of the factor $(1+\cos\theta)^2$ makes the last two cross sections vanish in the backward direction where $\cos\theta = -1$. This follows from the conservation of angular momentum. If the electron direction defines the $z$ axis, the initial state $e_L^-\mu_R^-$ has $J_z = -1$

Downloaded from https://www.cambridge.org/core. UNIVERSIDAD AUTONOMA METROPOLITANA, on 17 Nov 2026 at 09:09:05, subject to the Cambridge Core terms of use, available at https://www.cambridge.org/core/terms. https://doi.org/10.1017/9780511609923.010

because the spins are antiparallel to the $z$ axis and there is no orbital angular momentum along the direction of motion. For the final state $e_R^- \mu_L^-$ the same argument yields $J_z = +1$ if the scattering is at 180°. Thus the scattering must vanish in this configuration.

The connection between the center-of-mass scattering angle and the invariant variables used above is $1 + \cos\theta = 2(1 - y)$. The addition of the four separate electromagnetic processes produces the characteristic $1 + (1 - y)^2$ behavior found in the deep inelastic electron scattering formulas.

The analogous weak cross sections follow the same pattern, except that only the left-handed parts of the fermions and the right-handed parts of the antifermions participate in charged-current processes, thus

$$\frac{d\sigma}{d\Omega}(\nu_\mu e_L^- \to \mu_L^- \nu_e) = \frac{G_F^2 s}{2\pi^2}, \tag{8.27}$$

$$\frac{d\sigma}{d\Omega}(\nu_\mu \overline{\nu_e} \to \mu_L^- e_R^+) = \frac{G_F^2 s}{2\pi^2} \frac{(1 + \cos\theta)^2}{4}. \tag{8.28}$$

Using these simple formulas, we can determine the parton model values of the structure functions. Considering the scattering of a neutrino from a proton, we note that since the lepton loses charge ($\nu \to \mu^-$), the struck quark must gain charge. Thus it is only scattering from $d$ quarks or $\overline{u}$ quarks that contributes. In this way we find for $\nu_\mu p \to \mu^- X$ and $\overline{\nu}_\mu p \to \mu^+ X$

$$\frac{d\sigma^\nu}{dx\, dy} = \frac{2MEG_F^2}{\pi} x \left[ d(x) + (1 - y)^2 \overline{u}(x) \right], \tag{8.29}$$

$$\frac{d\sigma^{\overline{\nu}}}{dx\, dy} = \frac{2MEG_F^2}{\pi} x \left[ \overline{d}(x) + (1 - y)^2 u(x) \right]. \tag{8.30}$$

If the antiquarks, which are important only for rather small values of $x$, are ignored, the cross section for neutrino scattering is expected to be independent of $y$, while antineutrino scattering should vanish as $y \to 1$. To the extent to which the quark distributions are functions of $x$ alone, the total cross section, $\sigma$, and the mean value of the momentum transfer squared, $Q^2$, are both proportional to $E$.

Comparing with the general formula for neutrino scattering, we deduce the structure functions for neutrino scattering in the parton model:

$$F_1^\nu = d(x) + \overline{u}(x), \tag{8.31}$$

$$F_2^\nu = 2x[d(x) + \overline{u}(x)], \tag{8.32}$$

$$F_3^\nu = 2[d(x) - \overline{u}(x)], \tag{8.33}$$

$$F_1^{\overline{\nu}} = u(x) + \overline{d}(x), \tag{8.34}$$

$$F_2^{\overline{\nu}} = 2x[u(x) + \overline{d}(x)], \tag{8.35}$$

$$F_3^{\overline{\nu}} = 2[u(x) - \overline{d}(x)]. \tag{8.36}$$

Downloaded from https://www.cambridge.org/core. UNIVERSIDAD AUTONOMA METROPOLITANA, on 17 Nov 2026 at 09:09:05, subject to the Cambridge Core terms of use, available at https://www.cambridge.org/core/terms. https://doi.org/10.1017/9780511609923.010

If the target is an equal mixture of $u$ and $d$ quarks, as is nearly the case for neutrino experiments, except with a hydrogen bubble chamber, each occurrence of $u$ or $d$ gets replaced by the average of $u$ and $d$. Writing $q(x) = u(x) + d(x)$, $\overline{q}(x) = \overline{u}(x) + \overline{d}(x)$ we have

$$\frac{d\sigma^{\nu}}{dx\,dy} = \frac{MEG_F^2}{\pi} x\left[q(x) + (1-y)^2\overline{q}(x)\right] \tag{8.37}$$

$$\frac{d\sigma^{\overline{\nu}}}{dx\,dy} = \frac{MEG_F^2}{\pi} x\left[\overline{q}(x) + (1-y)^2 q(x)\right] \tag{8.38}$$

Actually, we should include strange quarks as well. For energetic neutrino beams we have the processes $\nu_\mu s \to \mu^- c$ and $\overline{\nu}_\mu \overline{s} \to \mu^+ \overline{c}$. Here $c$ is the charmed quark, to be discussed at length in Chapter 9. Our treatment has also been simplified by ignoring the Cabibbo angle.

The integrated cross sections are expressed in terms of $Q \equiv \int x\,dx\,q(x)$ and $\overline{Q} \equiv \int x\,dx\,\overline{q}(x)$, the momentum fractions carried by the quarks and the antiquarks.

$$\frac{d\sigma^{\nu}}{dy} = \frac{MEG_F^2}{\pi}\left[Q + (1-y)^2\overline{Q}\right]; \qquad \sigma^{\nu} = \frac{MEG_F^2}{\pi}\left[Q + \frac{1}{3}\overline{Q}\right]; \tag{8.39}$$

$$\frac{d\sigma^{\overline{\nu}}}{dy} = \frac{MEG_F^2}{\pi}\left[\overline{Q} + (1-y)^2 Q\right]; \qquad \sigma^{\overline{\nu}} = \frac{MEG_F^2}{\pi}\left[\overline{Q} + \frac{1}{3}Q\right]. \tag{8.40}$$

Since we expect much more of the momentum in the proton to be carried by the quarks than the antiquarks, we anticipate

$$\frac{\sigma^{\overline{\nu}}}{\sigma^{\nu}} \approx \frac{1}{3}. \tag{8.41}$$

Inserting the values of the constants, we find

$$\frac{\sigma^{\nu}}{E} = 1.56\left[Q + \frac{1}{3}\overline{Q}\right] 10^{-38}\ \text{cm}^2\ \text{GeV}^{-1}. \tag{8.42}$$

The total cross sections were measured at CERN using a heavy liquid (freon) bubble chamber, Gargamelle, which had been constructed at Orsay, near Paris (**Ref. 8.4**). Separate neutrino and antineutrino beams were generated by the CERN Proton Synchroton (PS). Outgoing muons were identified by their failure to undergo hadronic interactions in the bubble chamber. The energy of the produced hadronic system was measured by adding the energy of the charged particles measured in a 20-kG magnetic field, to the energy of the neutral pions observed through conversion of photons in the heavy liquid. The neutrino flux was monitored by measuring the muon flux associated with it.

While the Gargamelle data covered very low energies, $E_\nu < 10$ GeV, the expected linear behavior of the cross section on the neutrino energy was observed, with the results $\sigma^{\nu}/E = 0.74 \pm 0.02 \times 10^{-38}$ cm$^2$ GeV$^{-1}$, $\sigma^{\overline{\nu}}/E = 0.28 \pm 0.01 \times 10^{-38}$ cm$^2$ GeV$^{-1}$. These results were in good accord with the expectations.

Downloaded from https://www.cambridge.org/core. UNIVERSIDAD AUTONOMA METROPOLITANA, on 17 Nov 2026 at 09:09:05, subject to the Cambridge Core terms of use, available at https://www.cambridge.org/core/terms. https://doi.org/10.1017/9780511609923.010

The Gargamelle results were severely limited by the low energy of the CERN PS. Later studies were carried out at Fermilab by the Harvard, Penn, Wisconsin, and Fermilab Collaboration (HPWF) and the Caltech, Columbia, Fermilab, Rochester, and Rockefeller Collaboration (CCFRR) and at the CERN SPS by the CERN, Dortmund, Heidelberg, and Saclay Collaboration (CDHS) and the CERN, Hamburg, Amsterdam, Rome, and Moscow Collaboration (CHARM). Bubble chamber studies have also been done with the 15-foot bubble chamber at Fermilab and the Big European Bubble Chamber (BEBC) at CERN. The counter detectors have active target regions, calorimetry, and a muon spectrometer. These experiments confirmed the linearity of the cross section as a function of the neutrino energy and also gave similar results for $\sigma/E$, about $0.67 \times 10^{-38}\,\text{cm}^2\ \text{GeV}^{-1}$ for neutrinos and $0.34 \times 10^{-38}\text{cm}^2\ \text{GeV}^{-1}$ for antineutrinos.

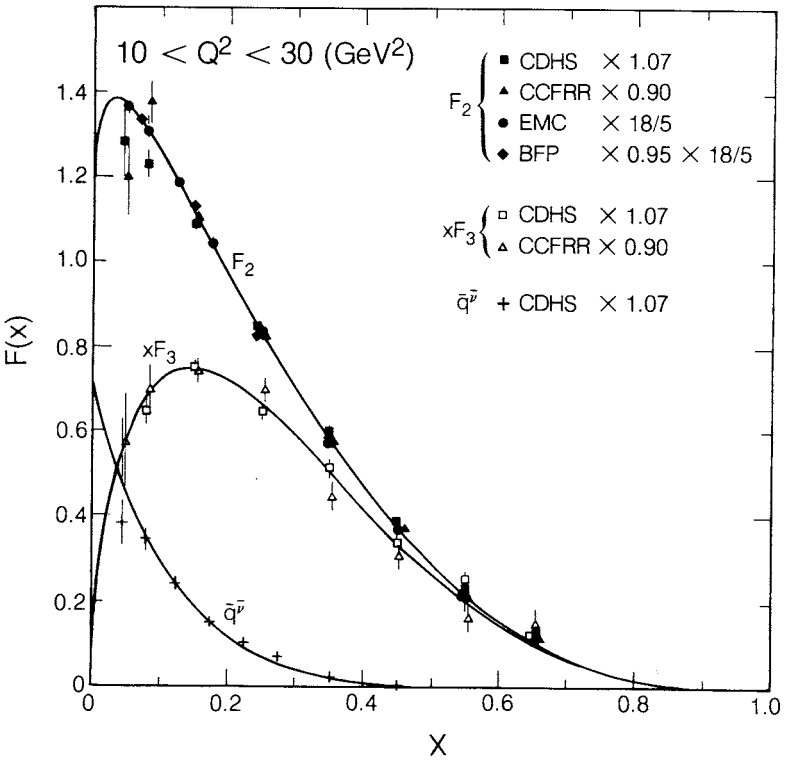



Figure 8.2. A compilation of data from neutrino and muon scattering experiments. The structure function $F_2$ is essentially proportional to the sum of the quark and antiquark distributions: $F_2(x) = x[q(x)+\overline{q}(x)]$. The structure function $xF_3$ is similarly related to the difference of the quark and antiquark distributions: $xF_3(x) = x[q(x) - \overline{q}(x)]$. The third combination shown is $\overline{q}^{\overline{\nu}}(x) = x[\overline{u}(x) + \overline{d}(x) + 2\overline{s}(x)]$. The data shown are from the CDHS, CCFRR, EMC (European Muon Collaboration), and BFP (Berkeley, Fermilab, Princeton) groups [compilation taken from *Review of Particle Properties*, *Phys. Lett.*, **170B**, 79 (1986)]. The normalizations of the data sets have been modified as indicated to bring them into better agreement. A factor 18/5, the inverse of the average charge squared of a light quark, is applied to the muon data to compare them with the neutrino data.

Downloaded from https://www.cambridge.org/core. UNIVERSIDAD AUTONOMA METROPOLITANA, on 17 Nov 2026 at 09:09:05, subject to the Cambridge Core terms of use, available at https://www.cambridge.org/core/terms. https://doi.org/10.1017/9780511609923.010

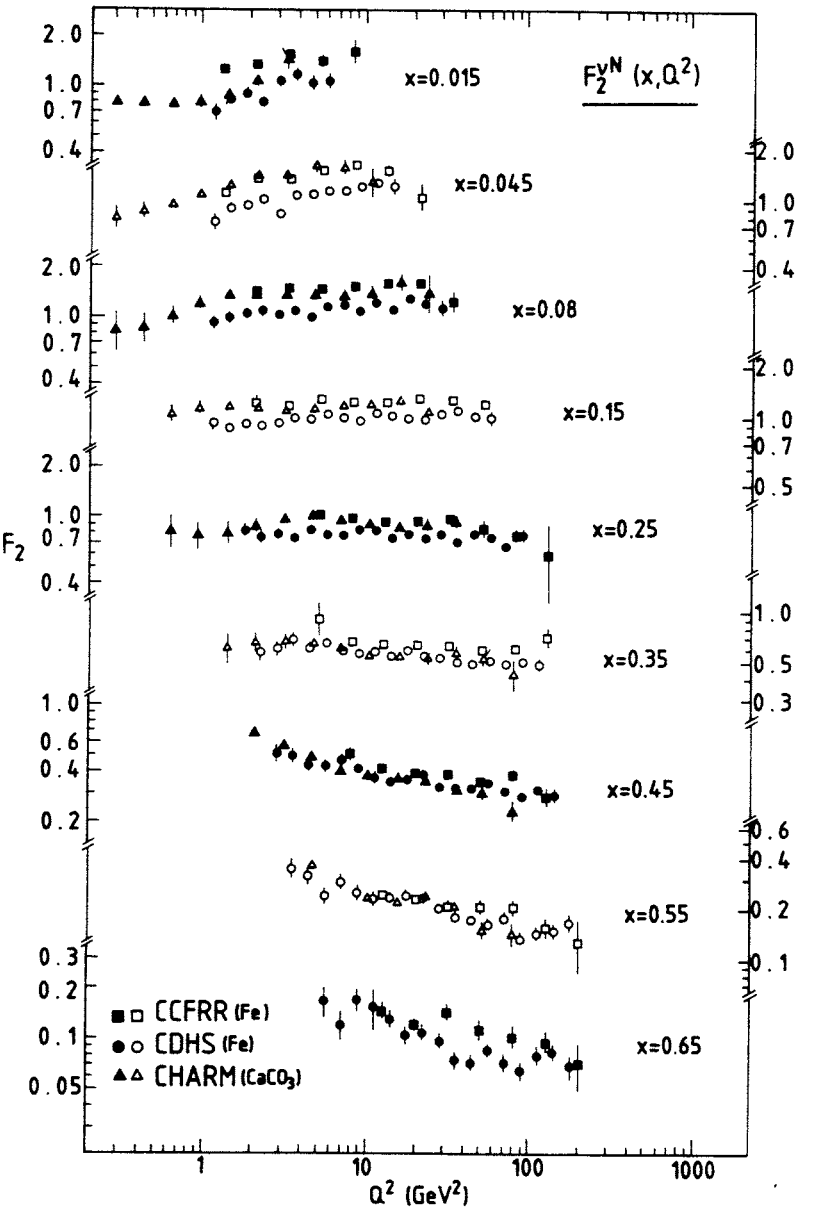



Figure 8.3. The structure functions $F_2$ for deep inelastic neutrino scattering as measured by the CDHS, CHARM and CCFRR collaborations. Scaling would require the structure functions to be independent of $Q^2$ at fixed $x$. The deviations seen from scaling are consistent with the predictions of QCD. From F. Dydak in *Proceedings of the 1983 International Lepton/Photon Symposium*, Cornell, 1983, p. 634.

Downloaded from https://www.cambridge.org/core. UNIVERSIDAD AUTONOMA METROPOLITANA, on 17 Nov 2026 at 09:09:05, subject to the Cambridge Core terms of use, available at https://www.cambridge.org/core/terms. https://doi.org/10.1017/9780511609923.010

The essence of the parton model is that the same quark distributions should work for all processes. For an isoscalar target, the electromagnetic structure function is

$$F_2 = \frac{5}{18}x(u + d + \overline{u} + \overline{d}) + \frac{1}{9}x(s + \overline{s}). \tag{8.43}$$

If the contribution from strange quarks is neglected, this is just 5/18 times the corresponding structure function for neutrinos on an isoscalar target. Neglecting the strange quarks is a good approximation for $x > 0.3$, where the antiquarks as well make a small contribution. The agreement between the electroproduction and neutrinoproduction data is satisfactory as is shown in Figure 8.2.

More detailed studies with electron, muon, and neutrino beams have demonstrated the $Q^2$ dependence predicted by QCD – the deviation from the scaling behavior of the "kindergarten" parton model. At high $x$, increasing $Q^2$ reduces the quark distribution because the quarks split into a quark and a gluon sharing the initial momentum, as described above. At low $x$, the structure functions increase as $Q^2$ increases because the momentum of high $x$ quarks is degraded by the emission process. These features are seen in Figure 8.3 showing data for $d\sigma/dy$ from the CDHS and CHARM collaborations at CERN and the CCFRR collaboration at Fermilab. The deviations from scaling provide indirect evidence for the existence of gluons. Direct evidence awaited the development of high-energy $e^+e^-$ colliding beam machines.

## Exercises

8.1 Verify the curves in Figure 5 of McAllister and Hofstadter.

8.2 What static charge distributions would produce the form factors $F(\mathbf{q}^2) = 1/(1 + \mathbf{q}^2/m^2)$ and $F(\mathbf{q}^2) = 1/(1 + \mathbf{q}^2/m^2)^2$?

8.3 We can define cross sections in the lab frame for virtual photons with momentum $q$ using polarization vectors $\epsilon_T$ and $\epsilon_L$, where $\epsilon \cdot q = 0$. If $q = (\nu, 0, 0, \sqrt{\nu^2 + Q^2})$, where $Q^2 = -q^2$, let

$$\epsilon_T = (0, 1, 0, 0)$$

$$\epsilon_L = (\sqrt{\nu^2 + Q^2}, 0, 0, \nu)/Q$$

so $\epsilon_T \cdot \epsilon_T = -1, \epsilon_L \cdot \epsilon_L = 1$. Then

$$\frac{\sigma_L}{\sigma_T} = \frac{\epsilon_L^\mu \epsilon_L^\nu W_{\mu\nu}}{\epsilon_T^\mu \epsilon_T^\nu W_{\mu\nu}}.$$

Show that

$$\frac{\sigma_L}{\sigma_T} = \frac{W_2}{W_1}\left(1 + \frac{\nu^2}{Q^2}\right) - 1.$$

Downloaded from https://www.cambridge.org/core. UNIVERSIDAD AUTONOMA METROPOLITANA, on 17 Nov 2026 at 09:09:05, subject to the Cambridge Core terms of use, available at https://www.cambridge.org/core/terms. https://doi.org/10.1017/9780511609923.010

8.4 * The deep inelastic scattering process has an amplitude that can be represented as

$$\mathcal{M} = \frac{e^2}{q^2}\overline{u}(k')\gamma_\mu u(k) < F|J^\mu(0)|p > .$$

Here $q = k - k'$ is the four-momentum transfer, and $k$ and $k'$ are the initial and final lepton momenta, $p$ is the initial nucleon momentum, and $|F >$ represents the final hadronic state. The cross section, summed over final states and averaged over initial lepton spins, is

$$d\sigma = \frac{(2\pi)^4}{4k\cdot p}\sum_F \delta^4(k + p - k' - p_F)\frac{d^3k'}{(2\pi)^3 2E'}$$
$$\times \prod_{\rm i}\frac{d^3p'_{\rm i}}{(2\pi)^3 2E'_{\rm i}}\left(\frac{4\pi\alpha}{q^2}\right)^2 \tfrac{1}{2}{\rm Tr}\not{k}'\gamma_\mu\not{k}\gamma_\nu < p|J^\nu(0)|F >< F|J^\mu(0)|p >$$

where $\not{k} = k_\mu\gamma^\mu$ and where we treat the lepton as massless. The $p'_{\rm i}$ represent final state momenta of the produced hadrons. We define

$$W^{\mu\nu} = \frac{1}{2M}(2\pi)^3\sum_F\int\prod_i\frac{d^3p'_{\rm i}}{(2\pi)^3 2E'_{\rm i}}\delta^4(p + q - p_F)$$
$$\times < p|J^\mu(0)|F >< F|J^\nu(0)|p > .$$

Current conservation requires that $q_\mu W^{\mu\nu} = q_\nu W^{\mu\nu} = 0$. The tensor $W^{\mu\nu}$ must be constructed from the vectors $p$ and $q$. Show that the most general form for $W^{\mu\nu}$ may be written as

$$W^{\mu\nu} = \left(-g^{\mu\nu} + \frac{q^\mu q^\nu}{q^2}\right)W_1 + \left(p^\mu - \frac{p\cdot q q^\mu}{q^2}\right)\left(p^\nu - \frac{p\cdot q q^\nu}{q^2}\right)W_2/M^2.$$

Show that

$$\frac{d\sigma}{dE'd\Omega'} = \frac{4\alpha^2E'^2}{Q^4}\left[2W_1\sin^2\tfrac{1}{2}\theta + W_2\cos^2\tfrac{1}{2}\theta\right]$$

where $\theta$ is the laboratory scattering angle of the lepton.

8.5 * If the sum defining $W_{\mu\nu}$ in Exercise 8.2 is restricted to elastic scattering, the Rosenbluth formula should be recovered. Demonstrate that this is so by taking

$$< F|J_\mu(0)|p > = \overline{u}(p')\left[F_1\gamma_\mu + iF_2\frac{\kappa q^\nu\sigma_{\mu\nu}}{2M}\right]u(p).$$

## Further Reading

A unique insight into the structure of the nucleon is found in the seminal *Photon-Hadron Interactions*, by R. P. Feynman, W. A. Benjamin, 1972.

Downloaded from https://www.cambridge.org/core. UNIVERSIDAD AUTONOMA METROPOLITANA, on 17 Nov 2026 at 09:09:05, subject to the Cambridge Core terms of use, available at https://www.cambridge.org/core/terms. https://doi.org/10.1017/9780511609923.010

A more theoretical discussion is given by C. Quigg in *Gauge Theories of the Strong, Weak, and Electromagnetic Interactions*, Benjamin/Cummings, Menlo Park, CA, 1983.

## References

**8.1** R. W. McAllister and R. Hofstadter, "Elastic Scattering of 188-MeV Electrons from the Proton and Alpha Particles." *Phys. Rev.*, **102**, 851 (1956).

**8.2** E. D. Bloom *et al.*, "High Energy Inelastic $e - p$ Scattering at $6^\circ$ and $10^\circ$." *Phys. Rev. Lett.*, **23**, 930 (1969).

**8.3** M. Breidenbach *et al.*, "Observed Behavior of Highly Inelastic Electron Proton Scattering." *Phys. Rev. Lett.*, **23**, 935 (1969). For scattering off neutrons, see also A. Bodek *et al.*, Phys. Rev. **D20**, 1471 (1979).

**8.4** T. Eichten *et al.*, "Measurement of the Neutrino-Nucleon and Anti Neutrino-Nucleon Total Cross Sections." *Phys. Lett.*, **46B**, 274 (1973).

Downloaded from https://www.cambridge.org/core. UNIVERSIDAD AUTONOMA METROPOLITANA, on 17 Nov 2026 at 09:09:05, subject to the Cambridge Core terms of use, available at https://www.cambridge.org/core/terms. https://doi.org/10.1017/9780511609923.010

PHYSICAL REVIEW VOLUME 102, NUMBER 3 MAY 1, 1956

# Elastic Scattering of 188-Mev Electrons from the Proton and the Alpha Particle*†‡§‖¶

R. W. McAllister and R. Hofstadter
*Department of Physics and High-Energy Physics Laboratory, Stanford University, Stanford, California*

(Received January 25, 1956)

The elastic scattering of 188-Mev electrons from gaseous targets of hydrogen and helium has been studied. Elastic profiles have been obtained at laboratory angles between 35° and 138°. The areas under such curves, within energy limits of ±1.5 Mev of the peak, have been measured and the results plotted against angle. In the case of hydrogen, a comparison has been made with the theoretical predictions of the Mott formula for elastic scattering and also with a modified Mott formula (due to Rosenbluth) taking into account both the anomalous magnetic moment of the proton and a finite size effect. The comparison shows that a finite size of the proton will account for the results and the present experiment fixes this size. The root-mean-square radii of charge and magnetic moment are each $(0.74\pm0.24)\times10^{-13}$ cm. In obtaining these results it is assumed that the usual laws of electromagnetic interaction and the Coulomb law are valid at distances less than $10^{-13}$ cm and that the charge and moment radii are equal. In helium, large effects of the finite size of the alpha-particle are observed and the rms radius of the alpha particle is found to be $(1.6\pm0.1)\times10^{-13}$ cm.

## I. INTRODUCTION

IN principle, it is possible to discover the finite size and structure of nuclei by methods of elastic electron scattering at high energies.[1–3] It is even possible to determine the structure of the proton by these methods.[4] For the light nuclei the Born approximation is adequate to analyze the experimental data, while for heavier nuclei such as gold or even copper[5] Yennie *et al.* have shown that a more accurate phase shift analysis is required.

The proton, deuteron, and alpha particle are most interesting to study because they are among the simplest nuclear structures. Furthermore, nuclei are built up out of protons and neutrons and it is fascinating to think of what the proton itself is built. In this paper we shall examine the structure of the proton and alpha particle. In an earlier paper[6] the scattering from the deuteron was reported.

## II. EXPERIMENTAL METHODS

Many of the experimental procedures have been reported in earlier papers.[2,3] The only important new variation over earlier methods has been the substitution of a gaseous target for the previously used metallic foils. The gaseous target will now be described.

In Fig. 1, the basic design of the target assembly is given. The cylinder is made of 410 stainless steel and has been heat-treated to increase its strength. The end plates are made of 0.010-inch stainless steel and are deformed by the high-pressure gases into the approximate shape shown in the figure. The target cylinder is $3\frac{1}{8}$ inches long and $\frac{3}{4}$ inch in diameter. The end plates are sealed by means of O-rings shown in the figure. Pressures as high as 2000 pounds per square inch have been used successfully in this chamber over long periods of time.

The geometry of the scattering experiment using the gaseous target chamber is shown in Fig. 2. Because of the double-focusing characteristic of the magnetic spectrometer and because of the defining slits at the entrance and exit of the spectrometer, the effective target viewed by the spectrometer has the appearance indicated schematically in Fig. 2. It is evident that to a very good approximation the scattering yield at any given angle will be proportional to the cosecant of the angle of observation in the laboratory system since the

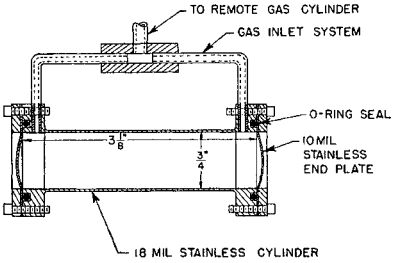



FIG. 1. Basic design of the gas chamber.

* The research reported in this document was supported jointly by the U. S. Navy (Office of Naval Research) and the U. S. Atomic Energy Commission, and by the U. S. Air Force through the Air Force Office of Scientific Research, Air Research and Development Command.

† Aided by a grant from the Research Corporation.

‡ These results were briefly reported at the Seattle Meeting of the American Physical Society, in July, 1954, but a comparison was not made at that time with the Rosenbluth results.

§ Miss Eva Wiener assisted in the early phases of this research. She was the victim of a fatal automobile accident in 1953.

‖ Some of the material now reported was published earlier in brief form, *viz.*, R. Hofstadter and R. W. McAllister, Phys. Rev. **98**, 217 (1955).

¶ *Note added in proof.*—Results more recent than those reported in this paper and extending to 550 Mev, were presented at the New York meeting of the American Physical Society [Bull. Am. Phys. Soc. Ser. II, 1 (1956)] by Hofstadter, Chambers, and Blankenbeder. The newer experiments confirm in greater detail the results presented in this paper. The newer results are being submitted for publication in *The Physical Review*.

[1] Hofstadter, Fechter, and McIntyre, Phys. Rev. **91**, 422 (1953).

[2] Hofstadter, Fechter, and McIntyre, Phys. Rev. **92**, 978 (1953).

[3] Hofstadter, Hahn, Knudsen, and McIntyre, Phys. Rev. **95**, 512 (1954).

[4] R. Hofstadter and R. W. McAllister, Phys. Rev. **98**, 217 (1955).

[5] Yennie, Wilson, and Ravenhall, Phys. Rev. **92**, 1325 (1953).

[6] J. A. McIntyre and R. Hofstadter, Phys. Rev. **98**, 158 (1954).



Downloaded from https://www.cambridge.org/core. UNIVERSIDAD AUTONOMA METROPOLITANA, on 17 Nov 2026 at 09:09:05, subject to the Cambridge Core terms of use, available at https://www.cambridge.org/core/terms. https://doi.org/10.1017/9780511609923.010

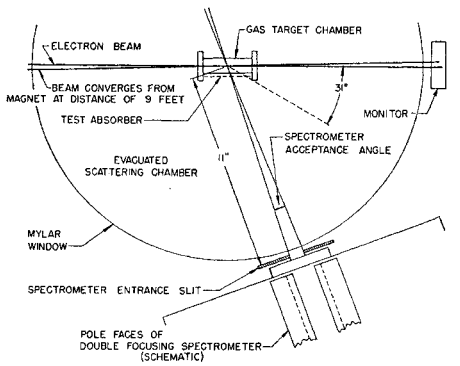



FIG. 2. Arrangement of parts in experiments on electron scattering from a gas target.

target thickness viewed by the spectrometer is proportional to this trigonometric function. Thus, to normalize the data to the same target thickness, the yield at any angle must be divided by the cosecant of the angle. In these experiments the effective target width viewed by the spectrometer is approximately $\frac{1}{2}$ inch at the gas chamber and this dimension is given by the vertical exit slit width (0.5 inch) imaged at the source.

The slit defining the acceptance angle in the plane common to the beam, scattering target, and entrance to the spectrometer, was $\frac{3}{4}$ inch wide and is indicated in Fig. 2. The exit collimator at the top of the magnet had a horizontal slit $\frac{5}{8}$ inch wide defining the energy band accepted by the Čerenkov detector, and a vertical slit $\frac{1}{2}$ inch wide. The vertical slit, together with the $\frac{3}{4}$ inch entrance slit, served to define the effective width of the target. In all the experiments herewith reported the incident beam was monochromatic within $\pm 1.0$ Mev in 187 Mev.

At small angles, that is, angles less than 30°, it is possible for the spectrometer to view the end walls of the chamber and thus accept spurious electrons scattered by the target end plates. At 35° and 40°, a small residual effect of this type is present and is always subtracted from the yield furnished by the gas plus the target chamber. In other words, the scattering intensity is measured first with the gas in the chamber and then again with the gas removed from the target. The latter measurement gives the "background" due to the end wall effects. At all other angles, this effect is negligible.

Multiple scattering and radiation straggling from the 0.018-inch cylinder walls introduce only minor errors at the angles studied. This has been determined empirically by inserting a 0.010-inch stainless steel test absorber in the position so marked in Fig. 2. The test absorber was placed in the path of electrons scattered at angles 50°, 90°, and 130°. Elastic profiles were measured with the test absorber in and out of the path. The peak of the elastic scattering profile was reduced 1 percent per mil of stainless steel in the direction of the scattered electrons, but the half-width of the curve was also increased by an amount such that the area under the elastic curve was the same, within 5 percent, whether the test absorber was in or out. This behavior may be understood as follows: The double focusing action of the spectrometer assures collection of all the electrons directed into the effective solid angle of the spectrometer, whether multiply-scattered or not and brings them to a focus beyond the energy slit (and from there into the Čerenkov detector). The only effects of multiple-scattering in the chamber walls are (a) to fuzz out the source of the scattered electrons in the gas, i.e., to increase or decrease the depth from which the scattered electrons appear to emerge from the target, (b) to reduce the angular resolution, and (c) to mix electrons scattered originally at different angles. Effect (a) may easily be seen to be of negligible importance. Effect (b) amounts to approximately $(\Delta\theta)_{\text{rms}}=\pm 1°$. Since the angular opening of the lower spectrometer slit is $\pm 2°$ and the multiple scattering is essentially Gaussian, the uncertainty in measuring the scattering angle is not appreciably increased by the effect of the side walls. The incoming end plate also contributes an uncertainty of $(\Delta\theta)_{\text{rms}}=\pm 0.7°$. The resulting uncertainty, combining all causes, is approximately $(\Delta\theta)_{\text{rms}}=\pm 2.4°$. The effect of multiple scattering in the hydrogen or helium gas volumes is of the order of 0.1° and hence negligible. In case (c), the error so introduced is of the order of tenths of a percent and is here neglected. In fact, plural scatterings are eliminated because of the energy selection of the spectrometer.

Radiation straggling of the electrons coming out through the walls of the chamber may be shown theoretically to contribute not more than a 5 percent relative correction between 50° and 90° and an equal figure between 90° and 130°, i.e., both the 50° yield and the 130° yield would each be lowered by something less than 5 percent with respect to the 90° yield. Our experiments with the test absorber have not demonstrated a consistent loss greater than 5 percent which could be attributed to straggling in the chamber walls. The statistical accuracy and drifts of the apparatus could have concealed an error of the order of 5 percent. Hence, we have not made a correction for straggling.

The lining-up procedure used a CsBr(Tl) crystal which could be moved remotely into or out of the beam. The crystal was placed along the beam axis just outside the scattering chamber. When it was desired to know the position of the beam, the crystal was moved into the beam and observed with a telescope. When the beam was lined up, say within $\pm\frac{1}{16}$ inch at the target, the crystal was withdrawn. Periodic checks showed whether or not the beam had moved. Very little beam motion was observed after an initial alignment.

An ion chamber was used in the early runs as a monitor of the incident beam, and a secondary electron

Downloaded from https://www.cambridge.org/core. UNIVERSIDAD AUTONOMA METROPOLITANA, on 17 Nov 2026 at 09:09:05, subject to the Cambridge Core terms of use, available at https://www.cambridge.org/core/terms. https://doi.org/10.1017/9780511609923.010

emitter[7] in the later runs. The ion chamber showed a small amount of saturation at large beams and its runs were corrected by the empirically determined calibration of ion chamber *versus* secondary electron emitter. No correction so obtained was larger than 10 percent. If the correction had not been included, the proton size (see below) would have been a trifle larger.

The theoretical Schwinger radiation correction has not been applied since its angular dependence is very weak and well within the statistics of our experimental observations.

## III. RESULTS

### A. Hydrogen

Typical elastic profiles observed in a run with hydrogen at an incident energy of 185 Mev are shown in Fig. 3. Because of recoil of the struck proton the energy of the elastically deflected electron is a decreasing function of the angle of scattering. This may be observed by noting the variable position of the peaks in Fig. 3. Figure 4 shows the theoretical behavior of the energy of the scattered electron plotted against laboratory scattering angle for an incident energy of 187 Mev. The solid points show the positions of the peaks of the elastic scattering curves taken at the various angular positions during an experimental run at 187 Mev. The agreement is excellent except at extreme angles where small deviations are observed. The deviations are actually expected because of an increasing energy loss in the wall as the angle of entry becomes more and more oblique. The observed reduction in energy of the scattered electrons below the theoretical curve is in good agreement with the energy loss in the wall.

Because of the variation in energy of the scattered electrons we have been concerned that the solid angle effective in collecting electrons could have been smaller at small angles (high energies), where magnet saturation is important, than at large angles (smaller energies), where saturation is less important. To test this possibility we have measured the number of scattered electrons as a function of the entrance slit width at both high (188 Mev) and low (139 Mev) energies. We have found that in both cases the number of scattered electrons for the $\frac{3}{4}$-inch entrance slit width is 15 percent below the number expected from the initial slope of the curve of number of scattered electrons *versus* slit width. The 15 percent reduction is due to the widest trajectories striking the magnet chamber walls. In the radial direction in the magnet no electrons are lost because of the small extent of the beam in this direction. In other words, the effective solid angle is the same at both low and high energies provided that the entrance slit width is not larger than $\frac{3}{4}$ inch. Hence correction for magnet saturation is not required.

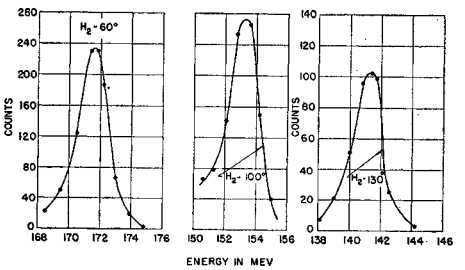



FIG. 3. Typical elastic profiles obtained with hydrogen gas at 185 Mev.

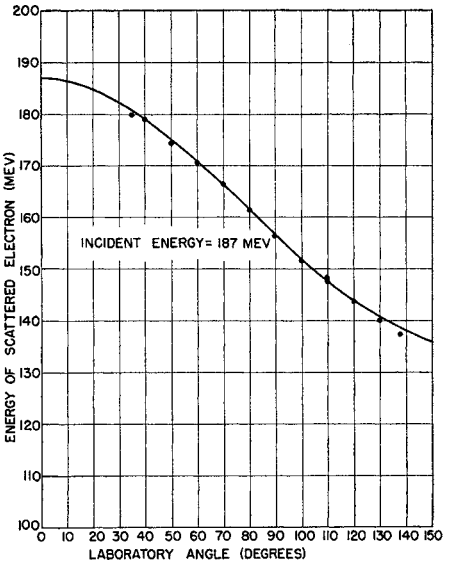



FIG. 4. The solid line gives the theoretical energy of the scattered electrons for an incident energy of 187 Mev. Relativistic kinematics are used to obtain the theoretical curve. The experimental points correspond to peak values of the elastic profiles and refer to experimental observations.

Areas under the elastic peaks, such as those of Fig. 3, have been measured by numerical integration over a width of $\pm 1.5$ Mev about the peak. Such values have been plotted against laboratory angle as in Fig. 5. Areas over $\pm 2$ and $\pm 2.5$ Mev widths have also been obtained by numerical integration, but the relative results are essentially the same. Only the $\pm 1.5$ Mev results will be presented below.

Figure 5 presents a summary of all the data obtained over a period of several months. It may be noticed that the experimental spread of points is somewhat larger than the statistical errors might lead one to expect. The causes of the spread are probably connected with small, unnoticed horizontal shifts of beam, hysteresis in the spectrometer magnet, small changes in the bias of the Čerenkov counter detection equipment, variations

[7] G. W. Tautfest and H. R. Fechter, Phys. Rev. **96**, 35 (1954); Rev. Sci. Instr. **26**, 229 (1955).

Downloaded from https://www.cambridge.org/core. UNIVERSIDAD AUTONOMA METROPOLITANA, on 17 Nov 2026 at 09:09:05, subject to the Cambridge Core terms of use, available at https://www.cambridge.org/core/terms. https://doi.org/10.1017/9780511609923.010

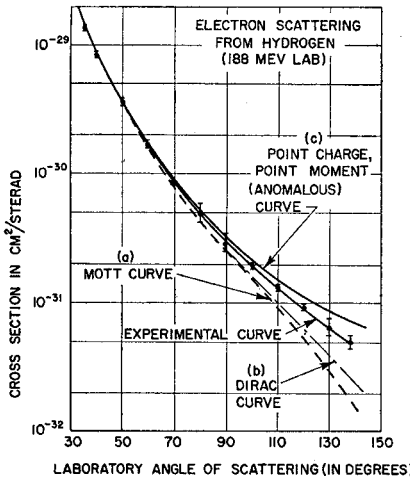



FIG. 5. Curve (a) shows the theoretical Mott curve for a spinless point proton. Curve (b) shows the theoretical curve for a point proton with the Dirac magnetic moment, curve (c) the theoretical curve for a point proton having the anomalous contribution in addition to the Dirac value of magnetic moment. The theoretical curves (b) and (c) are due to Rosenbluth.[8] The experimental curve falls between curves (b) and (c). This deviation from the theoretical curves represents the effect of a form factor for the proton and indicates structure within the proton, or alternatively, a breakdown of the Coulomb law. The best fit indicates a size of $0.70\times10^{-13}$ cm.

in saturation of the ion chamber monitor response and in the integrating voltmeter, and perhaps other unknown items. In Fig. 5 we have drawn a curve, labeled "experimental curve," which is our best estimate of the accumulated data at 188 Mev. The limits of error represent the greatest variations we have observed in any runs. However all runs, not being absolute, are normalized to each other by "best fitting." The experimental curve is also normalized to the theoretical curve at small angles. Also plotted in Fig. 5 are (a) the theoretical Mott curve for a spinless point proton, (b) the theoretical curve for a point proton with the Dirac value of magnetic moment (gyromagnetic ratio 2.00), (c) the theoretical curve for a point proton with the anomalous value of the proton moment in addition to the Dirac moment (gyromagnetic ratio=5.58). The theoretical curves (b), (c) are obtained from calculations of Rosenbluth.[8] The experimental curve deviates from curves (a), (b), and (c) at the larger angles and is lower than the curve for a point proton with anomalous moment, but higher than the curve for a point proton with Dirac moment. This reduction at large angles below the curve for point charge represents the effect of a "structure factor" or a "form factor" for the proton and hence indicates the finite size of the proton. Since the usual electromagnetic relations and the Coulomb interaction have been used in Rosenbluth's calculation, we are here assuming the validity of these interactions at small distances ($<10^{-13}$ cm). Subject to this assumption, the experiment indicates the proton is not a point.

In order to carry out the form factor calculations, we have made use of Rosenbluth's formalism.[8] However we have given the charge and magnetic moment phenomenological interpretations in place of the meson theoretic interpretations originally presented by Rosenbluth.[9] We may write Rosenbluth's formulas as follows: for a point charge we have

$$\sigma=\sigma_{NS}\left\{1+\frac{q^2}{4M^2}[2(1+\mu)^2\tan^2(\theta/2)+\mu^2]\right\}, \quad (1)$$

where

$$\sigma_{NS}=\frac{e^4}{4E^2}\left(\frac{\cos^2(\theta/2)}{\sin^4(\theta/2)}\right)\frac{1}{1+(2E/M)\sin^2(\theta/2)}, \quad (2)$$

and where

$$q=\frac{(2/\lambda)\sin(\theta/2)}{[1+(2E/M)\sin^2(\theta/2)]^{\frac{1}{2}}}. \quad (3)$$

Here natural units, $\hbar=c=1$, are used and the equations are written in terms of the laboratory coordinates; $q$ is the invariant momentum transfer in the center-of-mass frame expressed in laboratory coordinates; $E$ is the energy of the incident electrons; $M$ the mass of the proton, and $\mu$ is the anomalous part of the proton's magnetic moment ($\mu=1.79$). $\lambda$ is the reduced de Broglie wavelength of the electron in the laboratory system.

For a diffuse proton we may write:

$$\sigma=\sigma_{NS}\left\{F_1^2+\frac{q^2}{4M^2}[2(F_1+\mu F_2)^2\tan^2(\theta/2)+\mu^2F_2^2]\right\}, \quad (4)$$

where $F_1$ is the charge form factor (which also influences the intrinsic "Dirac" magnetic moment) and $F_2$ the anomalous magnetic moment form factor. In principle $F_1$ does not have to be the same as $F_2$. $F_1$ and $F_2$ may be written as functions of $(q\langle r\rangle)$, where $\langle r\rangle$ is the root-mean-square radius of the appropriate charge, or moment distribution. $F_1$ and $F_2$ may also be identified with $e'/e$ and $k'e'/k_0e$ in Rosenbluth's article.

We have not made detailed analyses for different $F_1$ and $F_2$. Rather, as may be seen below, we have assumed $F_1=F_2$. However, the data at all energies are quite consistent with this choice.

At the energies used in these experiments, the form factor ($F_1$ or $F_2$) is not appreciably shape dependent, i.e., one cannot distinguish between uniform, exponential, or Gaussian charge (or magnetic moment) distributions. All that can be determined is a mean square radius. Therefore we have tried to fit the experi-

[8] M. N. Rosenbluth, Phys. Rev. 79, 615 (1950).

[9] We are indebted to Dr. D. R. Yennie for formulation of Eqs. (1)–(4).

Downloaded from https://www.cambridge.org/core. UNIVERSIDAD AUTONOMA METROPOLITANA, on 17 Nov 2026 at 09:09:05, subject to the Cambridge Core terms of use, available at https://www.cambridge.org/core/terms. https://doi.org/10.1017/9780511609923.010

mental data with a phenomenological form factor corresponding to various values of the mean square radii up to values of $q\langle r\rangle \cong 1.0$. $q$ is again the momentum transfer and $\langle r\rangle$ the root-mean-square radius of the charge or magnetic moment distributions. For simplicity, as stated above, we have assumed that $\langle r\rangle_{\text{charge}} = \langle r\rangle_{\text{anomalous magnetic moment}}$, although in principle this is not a necessary restriction. Hence we can expect only to obtain a first approximation to the structure and size of the proton.

When such form factors are applied to the point charge-point moment curve, the behavior of the experimental curve can be reproduced very well. In fact for $\langle r\rangle_{\text{charge}} = \langle r\rangle_{\text{magnetic moment}} = 0.70\times10^{-13}$ the theoretical curve cannot be distinguished from the experimental curve within the limits of error. A separate theoretical curve for $0.70\times10^{-13}$ cm therefore has not been included in Fig. 5. The limits of error in the radius are conservatively estimated at $\pm0.24\times10^{-13}$ cm.

A similar fitting procedure can be employed with data obtained with electrons at 236 Mev in the incident beam. In this case our measurements could be made only at angles larger than or equal to 90° since our magnetic spectrometer cannot bend electrons of energy higher than those scattered at 90° (or smaller angles): For an incident energy of 236 Mev the scattered electron at 90° has an energy of 189 Mev, the approximate limit of our apparatus.

Figure 6 shows the experimental points obtained in several runs at 236 Mev. The shape of the point charge-point moment curve is shown as well as the experimental points. No absolute values are known for the experimental points so that the best that can be done is to try to fit the shape of the experimental curve with Eq. (4) for various values of $F_1$ and $F_2$. Again the assumption $F_1 = F_2$ is made. Such attempts are shown in Fig. 6 and are labeled rms 6.2, 7.8, and $9.3\times10^{-14}$ cm. The dotted curves corresponding to $6.2\times10^{-14}$ cm and $9.3\times10^{-14}$ cm may be shifted down or up respectively

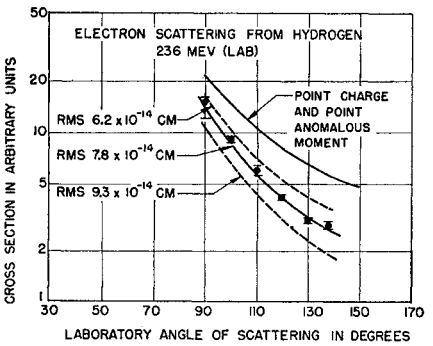



FIG. 6. This figure shows the experimental points at 236 Mev and the attempts to fit the shape of the experimental curve. The best fit lies near $0.78\times10^{-13}$ cm.

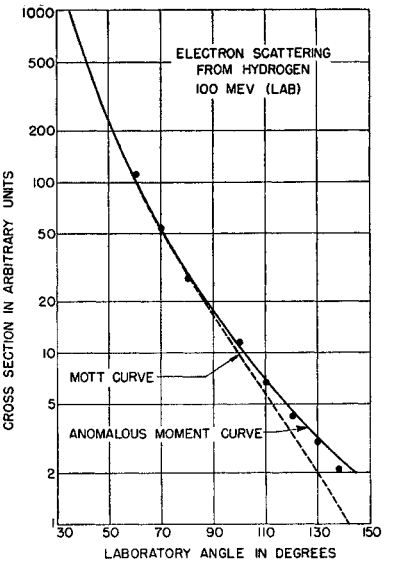



FIG. 7. Theoretical curves are shown for electrons of 100 Mev, along with the experimental observations at that energy.

to try to fit the experimental points, but neither curve will do so within the limits of error. Hence the data at 236 Mev support a "best" value of rms radius of $(0.78\pm0.20)\times10^{-13}$ cm, conservatively speaking. This value is in good agreement with the best value $(0.70\pm0.24)\times10^{-13}$ cm obtained above at 188 Mev.

In order to test some features of the apparatus, we have carried out a scattering experiment at an incident energy of 100 Mev. In this case, if our model of the proton is correct, the observed scattering should be quite close to the curve for a point charge and point moment because the $q\langle r\rangle$ value is small and $F^2 = 1.0$. Figure 7 shows that the agreement observed is highly satisfactory. At 100 Mev, the magnetic spectrometer is never saturated at any angle. Hence the "saturation" aspect and possible defocusing effects are not tested by this experiment. However, the 236-Mev and 188-Mev runs do test such possible effects since different energies correspond to different angular positions. The good agreement obtained between these latter two sets of data and the satisfactory behavior at 100 Mev is essentially what we have published earlier.[4]

These results may be summarized in the following way: If the proton can be assumed to (a) have distributions of charge and magnetic moment equal, or at least similar, in size and (b) if the Coulomb law and the usual electromagnetic laws are obeyed at distances of the order of $0.7\times10^{-13}$ cm, then these experiments show that the proton has an rms radius of $(0.74\pm0.24)\times10^{-13}$ cm. Of course, if the Coulomb law and the usual interactions are not valid, these findings could also be

Downloaded from https://www.cambridge.org/core. UNIVERSIDAD AUTONOMA METROPOLITANA, on 17 Nov 2026 at 09:09:05, subject to the Cambridge Core terms of use, available at https://www.cambridge.org/core/terms. https://doi.org/10.1017/9780511609923.010

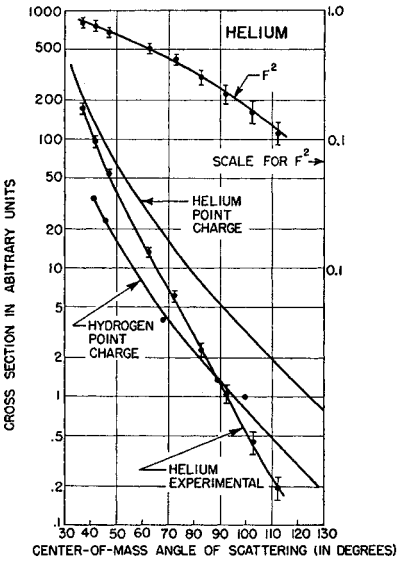



FIG. 8. The experimental curve for helium in the center-of-mass system, hydrogen normalizing points, and the helium point charge construction are shown. This figure also exhibits the square of the form factor as a function of angle. The best fit of theory to experiment corresponds to an rms radius of $1.60\times10^{-13}$ cm.

interpreted in terms of a point charge and point moment. We suspect that the breakdown of the Coulomb law would have exhibited other consequences, possibly already recognized in the literature. Phenomenologically we cannot distinguish, at the present time with these experiments alone, between a finite size of the proton and a breakdown of the Coulomb law. Nevertheless, any meson theory would predict a finite size of the proton's magnetic moment and this is what we may have found in the proton.

### B. Helium

The elastic peaks observed in helium are similar to those found in hydrogen, except that the recoil shifts are approximately four times smaller. To measure the form factor of the alpha particle with respect to electron scattering, we have made essentially simultaneous measurements of the scattering from helium and hydrogen and compared the results. The procedure involved carrying out the helium measurements, emptying the target chamber, and finally substitution of hydrogen for the helium. A series of measurements in hydrogen is thus made almost at the same time as the helium measurements. From a few representative hydrogen points, we can construct a point-charge *Mott curve* for hydrogen, say, between 35° and 90°. If we multiply this curve by four ($Z_{He}^2=2^2=4$) we obtain a theoretical point-charge curve for helium. Note that we use a Mott curve (spinless particle) since the alpha particle has no spin or magnetic moment. The ratio of the actually observed experimental curve in helium to the point charge curve for helium gives the square of the form factor. Thus the form factor can be compared with theoretical form factors for various size charge distributions.

Figure 8 shows the helium experimental curve in the center-of-mass system, the hydrogen normalizing points, and the helium point-charge construction. The incident energy was 188 Mev for these experiments. Corrections for the different energies in the center-of-mass system and for the different effective solid angles have been made. A glance at the figure shows that the elastic scattering from the alpha particle is considerably smaller at large angles (a factor of 10 at 110°) than that from a point charge.

Figure 8 also shows the ratio of the alpha-particle scattering to that of a point charge with $Z=2$. This curve represents the square of the "form factor." The scale is given in the upper right hand corner of Fig. 8. This curve is indistinguishable from a (form factor)$^2$ curve for an rms radius of $(1.60\pm0.10)\times10^{-13}$ cm. For such a small nucleus and an energy 188 Mev, our analysis will not give more than an rms radius from these measurements. It is curious that the rms radius of the alpha particle is approximately twice that of the proton as determined from these scattering measurements. Allowing for the rms radius of each of the two protons in the alpha particle, as determined above, the rms radius of the alpha particle would be smaller. By subtracting mean squares, the rms radius to the charge centroid would be $1.41\times10^{-13}$ cm. This approximate calculation probably overemphasizes the effect of the finite protonic size.

### ACKNOWLEDGMENTS

We wish to acknowledge the valuable cooperation of Mr. E. E. Chambers in helping with some of the measurements. We wish to thank Dr. R. H. Dalitz, Dr. D. G. Ravenhall, Dr. L. I. Schiff, and Dr. D. R. Yennie for many interesting conversations. We acknowledge with much appreciation the valued help of the late Miss Eva Wiener.

Downloaded from https://www.cambridge.org/core. UNIVERSIDAD AUTONOMA METROPOLITANA, on 17 Nov 2026 at 09:09:05, subject to the Cambridge Core terms of use, available at https://www.cambridge.org/core/terms. https://doi.org/10.1017/9780511609923.010

VOLUME 23, NUMBER 16 PHYSICAL REVIEW LETTERS 20 OCTOBER 1969

# HIGH-ENERGY INELASTIC $e$-$p$ SCATTERING AT 6° AND 10° *

E. D. Bloom, D. H. Coward, H. DeStaebler, J. Drees, G. Miller, L. W. Mo, and R. E. Taylor
Stanford Linear Accelerator Center, Stanford University, Stanford, California 94305

and

M. Breidenbach, J. I. Friedman, G. C. Hartmann,† and H. W. Kendall
Department of Physics and Laboratory for Nuclear Science,‡
Massachusetts Institute of Technology, Cambridge, Massachusetts 02139
(Received 19 August 1969)

Cross sections for inelastic scattering of electrons from hydrogen were measured for incident energies from 7 to 17 GeV at scattering angles of 6° to 10° covering a range of squared four-momentum transfers up to 7.4 $(\mathrm{GeV}/c)^2$. For low center-of-mass energies of the final hadronic system the cross section shows prominent resonances at low momentum transfer and diminishes markedly at higher momentum transfer. For high excitations the cross section shows only a weak momentum-transfer dependence.

Inelastic electron-proton scattering at high four-momentum transfer and large electron-energy loss has been used to investigate the electromagnetic structure and interactions of the proton.[1] We have measured the double differential cross section $d^2\sigma(E, E', \theta)/d\Omega dE'$ for electrons on hydrogen in a new kinematic region made accessible by the Stanford linear accelerator. We report measurements made at 6° and 10° for several incident energies $E$, and for a range of scattered energies $E'$, beginning at elastic scattering and ending at $E' \approx 3$ GeV. Only the scattered electron was detected. In this kind of measurement the two inelastic form factors[2] which describe the electromagnetic properties of the proton are functions of the squared four-momentum transfer, $q^2$, and the mass of the unobserved hadronic final state, $W$. We have measured several spectra at each angle to allow the calculation of model-independent radiative corrections[3] over a wide



Downloaded from https://www.cambridge.org/core. UNIVERSIDAD AUTONOMA METROPOLITANA, on 17 Nov 2026 at 09:09:05, subject to the Cambridge Core terms of use, available at https://www.cambridge.org/core/terms. https://doi.org/10.1017/9780511609923.010

range of $q^2$ and $W$.

We observe the excitation of several nucleon resonances[4-7] whose cross sections fall rapidly with increasing $q^2$. The region beyond $W \approx 2$ GeV exhibits a surprisingly weak $q^2$ dependence. This Letter describes the experimental procedure and reports cross sections for $W \geq 2$ GeV. Discussion of the results and a detailed description of the resonance region will follow.[8]

The incident energies at $\theta = 10°$ were 17.7, 15.2, 13.5, 11, and 7 GeV, and at $\theta = 6°$ were 16, 13.5, 10, and 7 GeV. For fixed $E$ and $\theta$, along a spectrum of decreasing $E'$, $W$ increases and $q^2$ decreases. The maximum range of these variables over a single measured spectrum occurred at an incident energy of 17.7 GeV and an angle of 10°, where $W$ varied from one proton mass to 5.2 GeV, and $q^2$ from 7.4 to 1.6 $(\mathrm{GeV}/c)^2$. For each spectrum $E'$ was changed in overlapping steps of 2% from elastic scattering, through the observed resonance region, to $W \approx 2$ GeV. Then steps corresponding to a change in $W$ of 0.5 GeV were made.

The electron beam from the accelerator was momentum analyzed with values of $\Delta p/p$ between $\pm 0.1$ and $\pm 0.25$% and then passed through a 7-cm liquid-hydrogen target. Two toroid charge monitors measured the integrated beam current with uncertainties of less than 0.5%. Electrons scattered in the target were momentum analyzed by a double-focusing magnetic spectrometer[9] capable of momentum analysis to 20 GeV/$c$. Particles selected by the spectrometer passed through a system of four hodoscopes to determine their trajectories and then into a pion-electron separation system based on the different cascade-shower properties of electrons and pions. This system considered of a 1-radiation-length slab of lead followed by three scintillation counters ($dE/dx$ counters) to detect showers initiated in the lead. The showers were then further developed in a total-absorption counter consisting of sixteen 1-radiation-length lead slabs alternated with Lucite Cherenkov counters. The $dE/dx$ counters increased the pion-electron separation efficiency by about a factor of 20 at lower $E'$, but were not required for values of $E'$ near the elastic peak. The electron-detection efficiency decreased with $E'$ and was 88% at 5 GeV. The uncertainty in the electron-detection efficiency was $\pm 1.5$% above $E' = 5$ GeV and increased to $\pm 4$% at $E' = 3$ GeV.

The momentum acceptance of the spectrometer was $\Delta p/p = 3.5$% with momentum resolution of 0.1%. The angular acceptance was $\Delta\theta = 7$ mrad with a resolution of 0.3 mrad. The measured solid angle of the instrument was $6 \times 10^{-5}$ sr with an uncertainty of $\pm 2$%.

Extensive tests showed that there could be significant reductions in target density due to beam heating. In order to correct for changes in the density a second spectrometer[10] was simultaneously used to measure protons from elastic electron-proton scattering at low momentum transfer. The angle and momentum settings of this spectrometer remained fixed for each spectrum. Usually the density reductions were less than 4%, with the maximum value being 13%. An uncertainty of $\pm 1$% was assigned to the measured cross sections for this correction.

The main trigger for an event was provided by a logical "or" between the total-absorption counter and a coincidence of two scintillation trigger counters placed before and after the hodoscopes. The event information was buffered and written on magnetic tape by a SDS-9300 on-line computer, which also provided preliminary on-line data analysis.

The cross sections were determined from an event-by-event analysis of the hodoscopes and the electron-pion discrimination counters. Corrections were made for fast-electronics and computer dead times, hodoscope-counter inefficiencies, multiple tracks, inefficiencies of electron identification, and target-density fluctuations. Yields from an empty replica of the experimental target, typically 7%, were subtracted from the full-target measurements. Electrons originating from $\pi^0$ decay and pair production were measured by reversing the spectrometer polarity and measuring positron yields. This correction is important only for small $E'$ and amounted to a maximum of 15%. The error associated with each point arose from counting statistics and uncertainties in electron-detection efficiencies, added in quadrature.

The data were analyzed separately at the Stanford Linear Accelerator Center (SLAC) and Massachusetts Institute of Technology (MIT) and averaged before each group began radiative corrections. The results of the analyses were in excellent agreement. For the results given in Table I, the two analyses differed from their mean by an average value of 0.35% with an rms deviation of 1.2%.

The radiative-correction procedures had two steps. The first was the subtraction of the calculated radiative tail of the elastic peak from each spectrum. Using the measured form factors



Downloaded from https://www.cambridge.org/core. UNIVERSIDAD AUTONOMA METROPOLITANA, on 17 Nov 2026 at 09:09:05, subject to the Cambridge Core terms of use, available at https://www.cambridge.org/core/terms. https://doi.org/10.1017/9780511609923.010

VOLUME 23, NUMBER 16 PHYSICAL REVIEW LETTERS 20 OCTOBER 1969

Table I. Measured cross sections for $W \geq 2.0$ GeV after all corrections. The errors are 1 standard deviation. The systematic error is not included in the table but is estimated at 5% for $E' > 5$ GeV, increasing to 10% at $E' \approx 3$ GeV.

| $\theta$ (deg) | E (GeV) | E' (GeV) | $q^2$ $(\mathrm{GeV}/c)^2$ | W (GeV) | $d^2\sigma/d\Omega dE'$ $(10^{-31}\ \mathrm{cm}^2/\mathrm{sr\text{-}GeV})$ |
|---|---|---|---|---|---|
| 6.000 | 7.000 | 5.130 | .393 | 2.000 | 21.5 ± .49 |
| | | 4.586 | .352 | 2.249 | 15.6 ± .40 |
| | | 3.750 | .287 | 2.587 | 9.33 ± .64 |
| | | 3.250 | .249 | 2.769 | 7.96 ± .73 |
| | 10.005 | 7.886 | .864 | 1.998 | 10.7 ± .23 |
| | | 7.349 | .806 | 2.249 | 9.24 ± .20 |
| | | 6.745 | .739 | 2.502 | 7.01 ± .27 |
| | | 5.361 | .587 | 3.001 | 4.97 ± .24 |
| | | 3.724 | .408 | 3.501 | 3.54 ± .30 |
| | 13.529 | 11.00 | 1.630 | 1.999 | 4.26 ± .087 |
| | | 10.48 | 1.553 | 2.249 | 4.10 ± .093 |
| | | 9.936 | 1.473 | 2.480 | 3.85 ± .056 |
| | | 8.512 | 1.262 | 3.004 | 2.79 ± .085 |
| | | 6.906 | 1.023 | 3.505 | 2.09 ± .11 |
| | | 5.054 | .749 | 4.004 | 1.85 ± .11 |
| | | 3.394 | .503 | 4.404 | 1.59 ± .27 |
| | 16.049 | 13.16 | 2.314 | 1.998 | 2.19 ± .042 |
| | | 12.64 | 2.222 | 2.250 | 2.21 ± .043 |
| | | 12.03 | 2.116 | 2.510 | 2.16 ± .042 |
| | | 10.69 | 1.880 | 3.008 | 1.84 ± .042 |
| | | 9.109 | 1.602 | 3.507 | 1.59 ± .056 |
| | | 7.282 | 1.280 | 4.006 | 1.24 ± .066 |
| | | 5.644 | .992 | 4.406 | 1.11 ± .074 |
| | | 3.851 | .677 | 4.805 | 1.13 ± .17 |
| 10.000 | 7.010 | 4.802 | 1.023 | 2.000 | 2.82 ± .090 |
| | | 4.294 | .915 | 2.250 | 2.34 ± .099 |
| | | 3.717 | .792 | 2.504 | 2.05 ± .12 |
| 10.000 | 10.988 | 7.915 | 2.643 | 2.001 | 5.66 ± .38 |
| | | 6.879 | 2.297 | 2.509 | 6.17 ± .27 |
| | | 5.634 | 1.881 | 3.008 | 5.59 ± .30 |
| | | 4.163 | 1.390 | 3.507 | 5.19 ± .43 |
| | | 3.000 | 1.001 | 3.856 | 5.38 ± .77 |
| | 13.534 | 9.737 | 4.004 | 2.000 | 1.80 ± .072 |
| | | 9.270 | 3.812 | 2.252 | 2.20 ± .083 |
| | | 8.737 | 3.593 | 2.508 | 2.62 ± .10 |
| | | 7.534 | 3.098 | 3.007 | 3.03 ± .15 |
| | | 6.113 | 2.514 | 3.506 | 2.93 ± .15 |
| | | 4.473 | 1.839 | 4.005 | 2.98 ± .25 |
| | | 3.000 | 1.234 | 4.406 | 3.75 ± .54 |
| | 15.201 | 10.86 | 5.016 | 2.002 | .876 ± .058 |
| | | 9.868 | 4.558 | 2.516 | 1.57 ± .060 |
| | | 8.691 | 4.014 | 3.014 | 1.94 ± .089 |
| | | 7.300 | 3.372 | 3.512 | 2.08 ± .083 |
| | | 5.696 | 2.631 | 4.011 | 1.98 ± .094 |
| | | 4.258 | 1.967 | 4.410 | 2.26 ± .15 |
| | | 3.700 | 1.709 | 4.555 | 2.17 ± .22 |
| | | 3.000 | 1.386 | 4.732 | 2.46 ± .28 |
| | 17.696 | 12.46 | 6.699 | 2.002 | .336 ± .020 |
| | | 11.50 | 6.184 | 2.514 | .617 ± .027 |
| | | 10.36 | 5.571 | 3.012 | .957 ± .042 |
| | | 9.015 | 4.847 | 3.510 | 1.19 ± .057 |
| | | 7.461 | 4.012 | 4.009 | 1.33 ± .073 |
| | | 6.069 | 3.263 | 4.408 | 1.32 ± .091 |
| | | 4.544 | 2.443 | 4.808 | 1.50 ± .15 |
| | | 3.800 | 2.043 | 4.991 | 1.70 ± .21 |
| | | 3.000 | 1.613 | 5.181 | 1.79 ± .37 |

for elastic electron-proton scattering, the radiative tail can be calculated to lowest order of $\alpha$ without using the peaking approximation.[11] Contributions from external and internal bremsstrahlung, including multiple photon emission, were calculated by two different methods. The differences between these methods were noticeable only for data with $E > 15$ GeV and $E' < 4$ GeV, and amounted to less than 2% in the corrected cross section. The maximum elastic-tail contributions to our data are 26% of the cross section at $E' = 3.8$ GeV in the 16-GeV, 6° spectrum and 21% at $E' = 3$ GeV in the 17.7-GeV, 10° spectrum.

The second step in the radiative correction procedure was a two-dimensional unfolding employing the peaking approximation.[11,12] All data at one angle were used to calculate the corrected cross sections. The computation involved no specific model for the cross section, but extensive interpolation and some extrapolation of the data were necessary. All experimental results having values of $E'$ greater than the lowest value



Downloaded from https://www.cambridge.org/core. UNIVERSIDAD AUTONOMA METROPOLITANA, on 17 Nov 2026 at 09:09:05, subject to the Cambridge Core terms of use, available at https://www.cambridge.org/core/terms. https://doi.org/10.1017/9780511609923.010

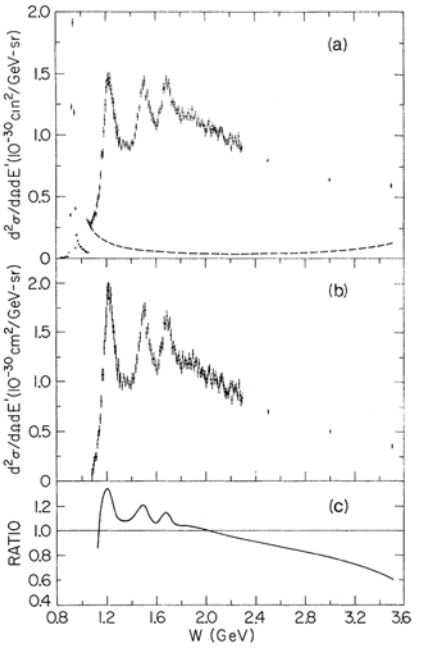



FIG. 1. The spectrum at $\theta = 6°$, $E = 10$ GeV (a) before and (b) after radiative corrections. In (a), the dashed line is the calculated elastic radiative tail which is subtracted before the two-dimensional unfolding is started. The elastic peak, but not the radiative tail, has been reduced by a factor of 6. (c) The ratio of the radiatively corrected to the uncorrected cross sections shown in (b) and (a). No systematic errors are shown. The radiative corrections increase the random errors.

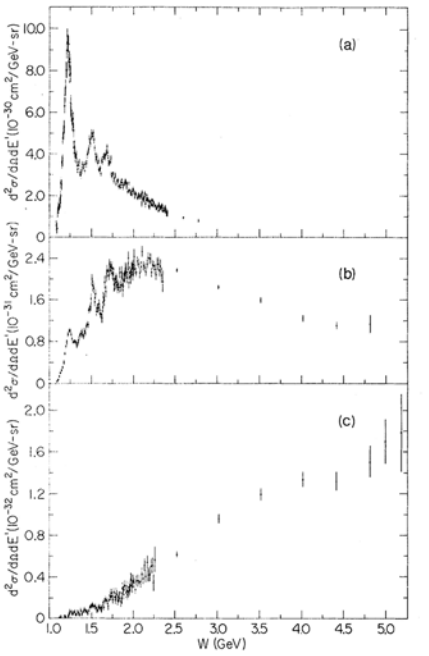



FIG. 2. Three representative radiatively corrected spectra at (a) $\theta = 6°$, $E = 7$ GeV; (b) $\theta = 6°$, $E = 16$ GeV, and (c) $\theta = 10°$, $E = 17.7$ GeV. The ranges of $q^2$ covered are (a) $0.2 \leq q^2 \leq 0.5$ (GeV/$c$)$^2$; (b) $0.7 \leq q^2 \leq 2.6$ (GeV/$c$)$^2$; and (c) $1.6 \leq q^2 \leq 7.3$ (GeV/$c$)$^2$. The elastic peaks are not shown.

of $E$ (7 GeV) utilized no extrapolated data. A variety of numerical procedures involving different kinematic contours for interpolation and extrapolation have been studied.

The errors of the measured cross sections were propagated through the radiative unfolding procedure. Additional uncertainties resulted from the numerical procedures and the approximations made in the application of the radiative correction theories. From various studies we believe that uncertainties due to interpolation techniques are less than 1%, and uncertainties due to extrapolation procedures (most important at the lowest $E$ spectrum at each angle) are less than 3%. Errors from theoretical approximations are more difficult to assess. They are small near the elastic peak and increase with decreasing $E'$; furthermore, they increase with increasing $\theta$. We believe that for these data, errors due to theoretical approximations are on the order of 5% or less.

The results of the MIT and SLAC analyses, which involved different radiative correction procedures, differed typically from their mean by less than 1%, and nowhere by more than $\frac{1}{2}$ a standard deviation. The results have been averaged, and the differences have been included in the estimate of systematic error.

Figure 1 shows the 10-GeV, 6° spectrum. Figure 1(a) is the spectrum before radiative corrections. The dashed line is the calculated elastic radiative-tail contribution to this spectrum. Figure 1(b) shows this spectrum after complete radiative corrections, and Fig. 1(c) shows the ratio of the corrected to the measured data. Figure 2 shows three other corrected spectra with progressively increasing ranges of $q^2$. The $q^2$ dependence of the inelastic continuum at large $W$ is clearly much weaker than that of the resonances.

Table I summarizes our results for $W \geq 2$ GeV. Data for $W \leq 2.3$ GeV are averages over a small



Downloaded from https://www.cambridge.org/core. UNIVERSIDAD AUTONOMA METROPOLITANA, on 17 Nov 2026 at 09:09:05, subject to the Cambridge Core terms of use, available at https://www.cambridge.org/core/terms. https://doi.org/10.1017/9780511609923.010

number of neighboring data points, and all other data represent averages over the total spectrometer acceptance. The kinematic variables correspond to the central ray of the spectrometer. The errors are 1 standard deviation based on counting statistics and electron-detection efficiency, propagated through the radiative correction programs. Systematic errors are not included in Table I. Estimates of the combined systematic errors are 5% for $E' > 5$ GeV increasing to 10% at $E' \approx 3$ GeV. These data are in general agreement, to within the stated errors, with the preliminary data reported at Vienna.[7]

We are pleased to acknowledge the assistance of R. Cottrell, C. Jordan, J. Litt, and S. Loken. Professor W. K. H. Panofsky, Professor J. Pine, and Professor B. Barish participated in the initial planning of the experiment. We are indebted to E. Taylor and the Spectrometer Facilities Group, and to the Technical Division under R. B. Neal, especially the Research Area and Accelerator Operations Departments. We appreciate the help of Mrs. E. Miller during the analysis.

---

*Work supported by the U. S. Atomic Energy Commission.

†Now at Xerox Corp., Rochester, N. Y.

‡Work supported in part by the Atomic Energy Commission under Contract No. AT(30-1)2098.

[1]J. D. Bjorken, in Selected Topics in Particle Physics, Proceedings of the International School of Physics "Enrico Fermi," Course XLI, edited by J. Steinberger (Academic Press, Inc., New York, 1968).

[2]For example, the inelastic cross section may be represented in terms of the form factors $W_1$ and $W_2$ as

$$\frac{d^2\sigma}{d\Omega dE'} = \frac{e^4 \cos^2\frac{1}{2}\theta}{4E^2 \sin^4\frac{1}{2}\theta}\left[W_2(q^2, W) + 2W_1(q^2, W)\tan^2\tfrac{1}{2}\theta\right].$$

The squared four-momentum transfer is $q^2 = 4EE' \times \sin^2\frac{1}{2}\theta$. The mass of the final hadronic state is $W = [M_p^2 + 2M_p(E - E') - q^2]^{1/2}$. $E$ and $E'$ are the incident- and scattered-electron energies and $\theta$ is the scattering angle, all in the laboratory frame. $M_p$ is the proton mass. For a discussion of the different form-factor notations see F. Gilman, Phys. Rev. 167, 1365 (1968).

[3]J. D. Bjorken, Ann. Phys. (N.Y.) 24, 201 (1963).

[4]A. A. Cone, K. W. Chen, J. R. Dunning, G. Hartwig, N. F. Ramsey, J. K. Walker, and R. Wilson, Phys. Rev. 156, 1490 (1967), and 163, 1854(E) (1967).

[5]F. W. Brasse, J. Engler, E. Ganssauge, and M. Schweizer, Nuovo Cimento 55A, 679 (1968).

[6]W. Bartel, B. Dudelzak, H. Krehbiel, J. McElroy, U. Meyer-Berkhout, W. Schmidt, V. Walther, and G. Weber, Phys. Letters 28B, 148 (1968).

[7]Preliminary results from the present experimental program are given in the report by W. K. H. Panofsky, in Proceedings of the Fourteenth International Conference on High Energy Physics, Vienna, Austria, September, 1968 (CERN Scientific Information Service, Geneva, Switzerland, 1968).

[8]See M. Breidenbach et al., following Letter [Phys. Rev. Letters 23, 935 (1969)] for a discussion of results. A description of the results obtained in the resonance region will be published.

[9]Brief descriptions of the spectrometer and the hodoscopes may be found in W. K. H. Panofsky, in Proceedings of the International Symposium on Electron and Photon Interactions at High Energies, Hamburg, Germany, 1965 (Springer-Verlag, Berlin, Germany, 1965), Vol. I; and A. M. Boyarski, F. Bulos, W. Busza, R. Diebold, S. D. Ecklund, G. E. Fischer, J. R. Rees, and B. Richter, Phys. Rev. Letters 20, 300 (1968).

[10]R. Anderson, D. Gustavson, R. Prepost, and D. Ritson, Nucl. Instr. Methods 66, 328 (1968).

[11]L. W. Mo and Y. S. Tsai, Rev. Mod. Phys. 41, 205 (1969).

[12]H. W. Kendall and D. Isabelle, Bull. Am. Phys. Soc. 9, 94 (1964).



Downloaded from https://www.cambridge.org/core. UNIVERSIDAD AUTONOMA METROPOLITANA, on 17 Nov 2026 at 09:09:05, subject to the Cambridge Core terms of use, available at https://www.cambridge.org/core/terms. https://doi.org/10.1017/9780511609923.010

VOLUME 23, NUMBER 16 PHYSICAL REVIEW LETTERS 20 OCTOBER 1969

# OBSERVED BEHAVIOR OF HIGHLY INELASTIC ELECTRON-PROTON SCATTERING

M. Breidenbach, J. I. Friedman, and H. W. Kendall
Department of Physics and Laboratory for Nuclear Science,*
Massachusetts Institute of Technology, Cambridge, Massachusetts 02139

and

E. D. Bloom, D. H. Coward, H. DeStaebler, J. Drees, L. W. Mo, and R. E. Taylor
Stanford Linear Accelerator Center,† Stanford, California 94305
(Received 22 August 1969)

Results of electron-proton inelastic scattering at 6° and 10° are discussed, and values of the structure function $W_2$ are estimated. If the interaction is dominated by transverse virtual photons, $\nu W_2$ can be expressed as a function of $\omega = 2M\nu/q^2$ within experimental errors for $q^2 > 1$ (GeV/$c$)$^2$ and $\omega > 4$, where $\nu$ is the invariant energy transfer and $q^2$ is the invariant momentum transfer of the electron. Various theoretical models and sum rules are briefly discussed.

In a previous Letter,[1] we have reported experimental results from a Stanford Linear Accelerator Center–Massachusetts Institute of Technology study of high-energy inelastic electron-proton scattering. Measurements of inelastic spectra, in which only the scattered electrons were detected, were made at scattering angles of 6° and 10° and with incident energies between 7 and 17 GeV. In this communication, we discuss some of the salient features of inelastic spectra in the deep continuum region.

One of the interesting features of the measurements is the weak momentum-transfer dependence of the inelastic cross sections for excitations well beyond the resonance region. This weak dependence is illustrated in Fig. 1. Here we have plotted the differential cross section divided by the Mott cross section, $(d^2\sigma/d\Omega dE')/(d\sigma/d\Omega)_{\mathrm{Mott}}$, as a function of the square of the four-momentum transfer, $q^2 = 2EE'(1-\cos\theta)$, for constant values of the invariant mass of the recoiling target system, $W$, where $W^2 = 2M(E-E') + M^2 - q^2$. $E$ is the energy of the incident electron, $E'$ is the energy of the final electron, and $\theta$ is the scattering angle, all defined in the laboratory system; $M$ is the mass of the proton. The cross section is divided by the Mott cross section

$$\left(\frac{d\sigma}{d\Omega}\right)_{\mathrm{Mott}} = \frac{e^4}{4E^2}\,\frac{\cos^2\tfrac{1}{2}\theta}{\sin^4\tfrac{1}{2}\theta}$$

in order to remove the major part of the well-known four-momentum transfer dependence arising from the photon propagator. Results from both 6° and 10° are included in the figure for each value of $W$. As $W$ increases, the $q^2$ dependence appears to decrease. The striking difference between the behavior of the inelastic and elastic cross sections is also illustrated in Fig. 1, where the elastic cross section, divided by the Mott cross section for $\theta = 10°$, is included. The $q^2$ dependence of the deep continuum is also consider-

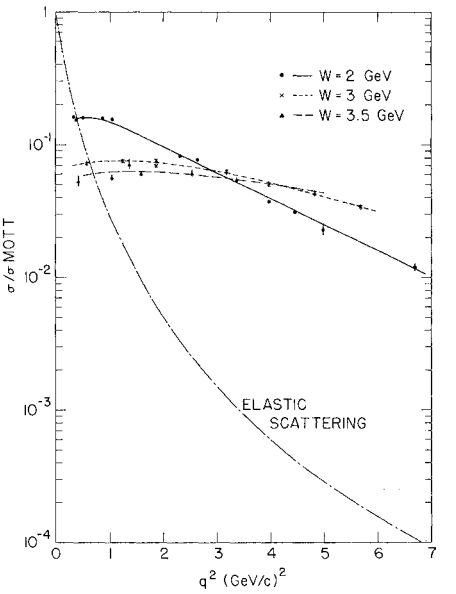



FIG. 1. $(d^2\sigma/d\Omega dE')/\sigma_{\mathrm{Mott}}$, in GeV$^{-1}$, vs $q^2$ for $W = 2$, 3, and 3.5 GeV. The lines drawn through the data are meant to guide the eye. Also shown is the cross section for elastic $e$–$p$ scattering divided by $\sigma_{\mathrm{Mott}}$, $(d\sigma/d\Omega)/\sigma_{\mathrm{Mott}}$, calculated for $\theta = 10°$, using the dipole form factor. The relatively slow variation with $q^2$ of the inelastic cross section compared with the elastic cross section is clearly shown.



Downloaded from https://www.cambridge.org/core. UNIVERSIDAD AUTONOMA METROPOLITANA, on 17 Nov 2026 at 09:09:05, subject to the Cambridge Core terms of use, available at https://www.cambridge.org/core/terms. https://doi.org/10.1017/9780511609923.010

VOLUME 23, NUMBER 16 PHYSICAL REVIEW LETTERS 20 OCTOBER 1969

ably weaker than that of the electroexcitation of the resonances,[2] which have a $q^2$ dependence similar to that of elastic scattering for $q^2 > 1$ (GeV/$c$)$^2$.

On the basis of general considerations, the differential cross section for inelastic electron scattering in which only the electron is detected can be represented by the following expression[3]:

$$\frac{d^2\sigma}{d\Omega dE'} = \left(\frac{d\sigma}{d\Omega}\right)_{\text{Mott}} (W_2 + 2W_1 \tan^2\tfrac{1}{2}\theta).$$

The form factors $W_2$ and $W_1$ depend on the properties of the target system, and can be represented as functions of $q^2$ and $\nu = E - E'$, the electron energy loss. The ratio $W_2/W_1$ is given by

$$\frac{W_2}{W_1} = \left(\frac{q^2}{\nu^2 + q^2}\right)(1+R), \quad R \geq 0,$$

where $R$ is the ratio of the photoabsorption cross sections of longitudinal and transverse virtual photons, $R = \sigma_S/\sigma_T$.[4]

The objective of our investigations is to study the behavior of $W_1$ and $W_2$ to obtain information about the structure of the proton and its electromagnetic interactions at high energies. Since at present only cross-section measurements at small angles are available, we are unable to make separate determinations of $W_2$ and $W_1$. However, we can place limits on $W_2$ and study the behavior of these limits as a function of the invariants $\nu$ and $q^2$.

Bjorken[5] originally suggested that $W_2$ could have the form

$$W_2 = (1/\nu)F(\omega),$$

where

$$\omega = 2M\nu/q^2.$$

$F(\omega)$ is a universal function that is conjectured to be valid for large values of $\nu$ and $q^2$. This function is universal in the sense that it manifests scale invariance, that is, it depends only on the ratio $\nu/q^2$. Since

$$\nu W_2 = \frac{\nu d^2\sigma/d\Omega\, dE'}{(d\sigma/d\Omega)_{\text{Mott}}}\left[1 + 2\frac{1}{1+R}\left(1 + \frac{\nu^2}{q^2}\right)\tan^2\tfrac{1}{2}\theta\right]^{-1},$$

the value of $\nu W_2$ for any given measurement clearly depends on the presently unknown value of $R$. It should be noted that the sensitivity to $R$ is small when $2(1+\nu^2/q^2)\tan^2\tfrac{1}{2}\theta \ll 1$. Experimental limits on $\nu W_2$ can be calculated on the basis of the extreme assumptions $R = 0$ and $R = \infty$. In Figs. 2(a) and 2(b) the experimental values of $\nu W_2$

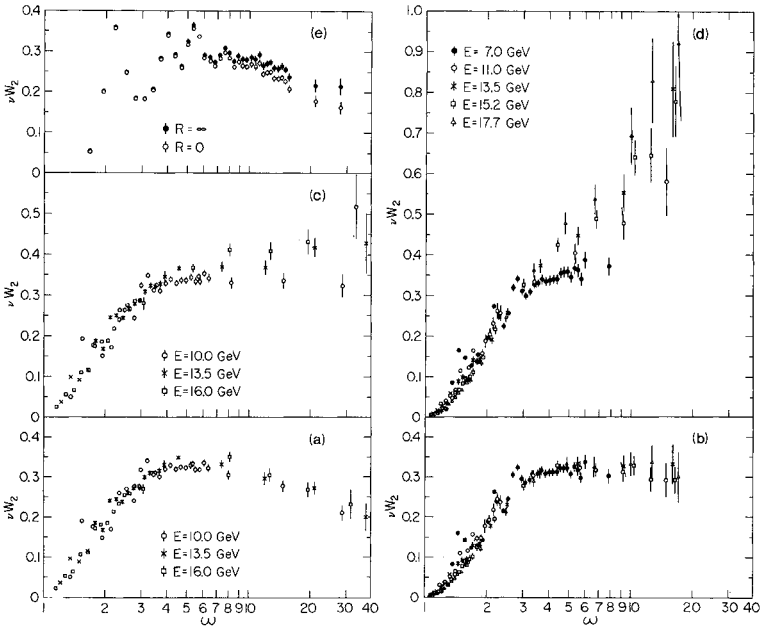



FIG. 2. $\nu W_2$ vs $\omega = 2M\nu/q^2$ is shown for various assumptions about $R = \sigma_S/\sigma_T$. (a) 6° data except for 7-GeV spectrum for $R = 0$. (b) 10° data for $R = 0$. (c) 6° data except for 7-GeV spectrum for $R = \infty$. (d) 10° data for $R = \infty$. (e) 6°, 7-GeV spectrum for $R = 0$ and $R = \infty$.



Downloaded from https://www.cambridge.org/core. UNIVERSIDAD AUTONOMA METROPOLITANA, on 17 Nov 2026 at 09:09:05, subject to the Cambridge Core terms of use, available at https://www.cambridge.org/core/terms. https://doi.org/10.1017/9780511609923.010

from the 6° and 10° data for $q^2 > 0.5$ (GeV/$c$)$^2$ are shown as a function of $\omega$ for the assumption that $R = 0$. Figures 2(c) and 2(d) show the experimental values of $\nu W_2$ calculated from the 6° and 10° data with $q^2 > 0.5$ (GeV/$c$)$^2$ under the assumption $R = \infty$. The 6°, 7-GeV results for $\nu W_2$, all of which have values of $q^2 \leq 0.5$ (GeV/$c$)$^2$, are shown for both assumptions in Fig. 2(e). The elastic peaks are not displayed in Fig. 2.

The results shown in these figures indicate the following:

(1) If $\sigma_T \gg \sigma_S$, the experimental results are consistent with a universal curve for $\omega \gtrsim 4$ and $q^2 \gtrsim 0.5$ (GeV/$c$)$^2$. Above these values, the measurements at 6° and 10° give the same results within the errors of measurements. The 6°, 7-GeV measurements of $\nu W_2$, all of which have values of $q^2 \leq 0.5$ (GeV/$c$)$^2$, are somewhat smaller than the results from the other spectra in the continuum region.

The values of $\nu W_2$ for $\omega \gtrsim 5$ show a gradual decrease as $\omega$ increases. In order to test the statistical significance of the observed slope, we have made linear least-squares fits to the values of $\nu W_2$ in the region $6 \leq \omega \lesssim 25$. These fits give $\nu W_2 = (0.351 \pm 0.023) - (0.003\,86 \pm 0.000\,88)\omega$ for data with $q^2 > 0.5$ (GeV/$c$)$^2$ and $\nu W_2 = (0.366 \pm 0.024) - (0.0045 \pm 0.0019)\omega$ for $q^2 > 1$ (GeV/$c$)$^2$. The quoted errors consist of the errors from the fit added in quadrature with estimates of systematic errors.

Since $\sigma_T + \sigma_S \simeq 4\pi^2 \alpha \nu W_2 / q^2$ for $\omega \gg 1$, our results can provide information about the behavior of $\sigma_T$ if $\sigma_T \gg \sigma_S$. The scale invariance found in the measurements of $\nu W_2$ indicates that the $q^2$ dependence of $\sigma_T$ is approximately $1/q^2$. The gradual decrease exhibited in $\nu W_2$ for large $\omega$ suggests that the photoabsorption cross section for virtual photons falls slowly at constant $q^2$ as the photon energy $\nu$ increases.

The measurements indicate that $\nu W_2$ has a broad maximum in the neighborhood of $\omega = 5$. The question of whether this maximum has any correspondence to a possible quasielastic peak[6] requires further investigation.

It should be emphasized that all of the above conclusions are based on the assumption that $\sigma_T \gg \sigma_S$.

(2) If $\sigma_S \gg \sigma_T$, the measurements of $\nu W_2$ do not follow a universal curve and have the general feature that at constant $2M\nu/q^2$, the value of $\nu W_2$ increases with $q^2$.

(3) For either assumption, $\nu W_2$ shows a threshold behavior in the range $1 \leq \omega \lesssim 4$. $W_2$ is constrained to be zero at inelastic threshold which corresponds to $\omega \simeq 1$ for large $q^2$. In the threshold region of $\nu W_2$, $W_2$ falls rapidly as $q^2$ increases at constant $\nu$. This qualitatively different from the weak $q^2$ behavior for $\omega > 4$. For $q^2 \approx 1$ (GeV/$c$)$^2$, the threshold region contains the resonances excited in electroproduction. As $q^2$ increases, the variations due to these resonances damp out and the values of $\nu W_2$ do not appear to vary rapidly with $q^2$ at constant $\omega$.

It can be seen from a comparison of Figs. 2(a) and 2(c) that the 6° data provide a measurement of $\nu W_2$ to within 10% up to a value of $\omega \approx 6$, irrespective of the values of $R$.

There have been a number of different theoretical approaches in the interpretation of the high-energy inelastic electron-scattering results. One class of models,[6-9] referred to as parton models, describes the electron as scattering incoherently from pointlike constituents within the proton. Such models lead to a universal form for $\nu W_2$, and the point charges assumed in specific models give the magnitude of $\nu W_2$ for $\omega > 2$ to within a factor of 2.[6] Another approach[10,11] relates the inelastic scattering to off-the-mass-shell Compton scattering which is described in terms of Regge exchange using the Pomeranchuk trajectory. Such models lead to a flat behavior of $\nu W_2$ as a function of $\nu$ but do not require the weak $q^2$ dependence observed and do not make any numerical predictions at this time. Perhaps the most detailed predictions made at present come from a vector-dominance model which primarily utilizes the $\rho$ meson.[12] This model reproduces the gross behavior of the data and has the feature that $\nu W_2$ asymptotically approaches a function of $\omega$ as $q^2 \to \infty$. However, a comparison of this model with the data leads to statistically significant discrepancies. This can be seen by noting that the prediction for $d^2\sigma/d\Omega dE'$ contains a parameter $\xi$, the ratio of the cross sections for longitudinally and transversely polarized $\rho$ mesons on protons, which is expected to be a function of $W$ but which should be independent of $q^2$. For values of $W \geq 2$ GeV, the experimental values of $\xi$ increase by about $(50 \pm 5)$% as $q^2$ increases from 1 to 4 (GeV/$c$)$^2$. This model predicts that

$$\sigma_S/\sigma_T = \xi(W)(q^2/m_\rho{}^2)[1 - q^2/2m\nu],$$

which will provide the most stringent test of this approach when a separation of $W_1$ and $W_2$ can be made.

The application of current algebra[13-17] and the use of current commutators leading to sum rules



Downloaded from https://www.cambridge.org/core. UNIVERSIDAD AUTONOMA METROPOLITANA, on 17 Nov 2026 at 09:09:05, subject to the Cambridge Core terms of use, available at https://www.cambridge.org/core/terms. https://doi.org/10.1017/9780511609923.010

and sum-rule inequalities provide another way of comparing the measurements with theory. There have been some recent theoretical considerations[18-20] which have pointed to possible ambiguity in these calculations; however, it is still of considerable interest to compare them with experiment.

In general, $W_2$ and $W_1$ can be related to commutators of electromagnetic current densities.[6,16] The experimental value of the energy-weighted sum $\int_1^\infty (d\omega/\omega^2)(\nu W_2)$, which is related to the equal-time commutator of the current and its time derivative, is $0.16 \pm 0.01$ for $R = 0$ and $0.20 \pm 0.03$ for $R = \infty$. The integral has been evaluated with an upper limit $\omega = 20$. This integral is also important in parton theories where its value is the mean square charge per parton.

Gottfried[21] has calculated a constant-$q^2$ sum rule for inelastic electron-proton scattering based on a nonrelativistic quark model involving pointlike quarks. The resulting sum rule is

$$\int_1^\infty \frac{d\omega}{\omega}(\nu W_2) = \int_{q^2/2M}^\infty d\nu W_2 = 1 - \frac{G_{Ep}^2 + (q^2/4M^2)G_{Mp}}{1 + q^2/4M^2},$$

where $G_{Ep}$ and $G_{Mp}$ are the electric and magnetic form factors of the proton. The experimental evaluation of this integral from our data is much more dependent on the assumption about $R$ than the previous integral. We will thus use the 6° measurements of $W_2$ which are relatively insensitive to $R$. Our data for a value of $q^2 \simeq 1$ (GeV/$c$)$^2$, which extend to a value of $\nu$ of about 10 GeV, give a sum that is $0.72 \pm 0.05$ with the assumption that $R = 0$. For $R = \infty$, its value is $0.81 \pm 0.06$. An extrapolation of our measurements of $\nu W_2$ for each assumption suggests that the sum is saturated in the region $\nu \simeq 20$-$40$ GeV. Bjorken[13] has proposed a constant-$q^2$ sum-rule inequality for high-energy scattering from the proton and neutron derived on the basis of current algebra. His result states that

$$\int_1^\infty \frac{d\omega}{\omega}\nu(W_{2p} + W_{2n}) = \int_{q^2/2M}^\infty d\nu(W_{2p} + W_{2n}) \geq \tfrac{1}{2},$$

where the subscripts $p$ and $n$ refer to the proton and neutron, respectively. Since there are presently no electron-neutron inelastic scattering results available, we estimate $W_{2n}$ in a model-dependent way. For a quark model[22] of the proton, $W_{2n} \simeq 0.8 W_{2p}$ whereas in the model[8] of Drell and co-workers, $W_{2n}$ rapidly approaches $W_{2p}$ as $\nu$ increases. Using our results, this inequality is just satisfied at $\omega \simeq 4.5$ for the quark model and at $\omega \simeq 4.0$ for the other model for either assumption about $R$. For example, this corresponds to a value of $\nu \simeq 4.5$ GeV for $q^2 = 2$ (GeV/$c$)$^2$. Bjorken[23] estimates that the experimental value of the sum is too small by about a factor of 2 for either model, but is should be noted that the $q^2$ dependence found in the data is consistent with the predictions of this calculation.

---

*Work supported in part through funds provided by the U. S. Atomic Energy Commission under Contract No. AT(30-1)2098.

†Work supported by the U. S. Atomic Energy Commission.

[1]E. Bloom et al., preceding Letter [Phys. Rev. Letters 23, 930 (1969)].

[2]Preliminary results from the present experimental program are given in the report by W. K. H. Panofsky, in Proceedings of the Fourteenth International Conference On High Energy Physics, Vienna, Austria, 1968 (CERN Scientific Information Service, Geneva, Switzerland, 1968), p. 23.

[3]R. von Gehlen, Phys. Rev. 118, 1455 (1960); J. D. Bjorken, 1960 (unpublished); M. Gourdin, Nuovo Cimento 21, 1094 (1961).

[4]See L. Hand, in Proceedings of the Third International Symposium on Electron and Photon Interactions at High Energies, Stanford Linear Accelerator Center, Stanford, California, 1967 (Clearing House of Federal Scientific and Technical Information, Washington, D. C., 1968), or F. J. Gilman, Phys. Rev. 167, 1365 (1968).

[5]J. D. Bjorken, Phys. Rev. 179, 1547 (1969).

[6]J. D. Bjorken and E. A. Paschos, Stanford Linear Accelerator Center, Report No. SLAC-PUB-572, 1969 (to be published).

[7]R. P. Feynman, private communication.

[8]S. J. Drell, D. J. Levy, and T. M. Yan, Phys. Rev. Letters 22, 744 (1969).

[9]K. Huang, in Argonne National Laboratory Report No. ANL-HEP 6909, 1968 (unpublished), p. 150.

[10]H. D. Abarbanel and M. L. Goldberger, Phys. Rev. Letters 22, 500 (1969).

[11]H. Harari, Phys. Rev. Letters 22, 1078 (1969).

[12]J. J. Sakurai, Phys. Rev. Letters 22, 981 (1969).

[13]J. D. Bjorken, Phys. Rev. Letters 16, 408 (1966).

[14]J. D. Bjorken, in Selected Topics in Particle Physics, Proceedings of the International School of Physics "Enrico Fermi," Course XLI, edited by J. Steinberger (Academic Press, Inc., New York, 1968).

[15]J. M. Cornwall and R. E. Norton, Phys. Rev. 177, 2584 (1969).

[16]C. G. Callan, Jr., and D. J. Gross, Phys. Rev. Letters 21, 311 (1968).

[17]C. G. Callan, Jr., and D. J. Gross, Phys. Rev. Letters 22, 156 (1969).



Downloaded from https://www.cambridge.org/core. UNIVERSIDAD AUTONOMA METROPOLITANA, on 17 Nov 2026 at 09:09:05, subject to the Cambridge Core terms of use, available at https://www.cambridge.org/core/terms. https://doi.org/10.1017/9780511609923.010

[18]R. Jackiw and G. Preparata, Phys. Rev. Letters 22, 975 (1969).
[19]S. L. Adler and W.-K. Tung, Phys. Rev. Letters 22, 978 (1969).
[20]H. Cheng and T. T. Wu, Phys. Rev. Letters 22, 1409 (1969).
[21]K. Gottfried, Phys. Rev. Letters 18, 1174 (1967).
[22]J. D. Bjorken, Stanford Linear Accelerator Center, Report No. SLAC-PUB-571, 1969 (unpublished).
[23]J. D. Bjorken, private communication.



Downloaded from https://www.cambridge.org/core. UNIVERSIDAD AUTONOMA METROPOLITANA, on 17 Nov 2026 at 09:09:05, subject to the Cambridge Core terms of use, available at https://www.cambridge.org/core/terms. https://doi.org/10.1017/9780511609923.010

Volume 46B, number 2 PHYSICS LETTERS 17 September 1973

# MEASUREMENT OF THE NEUTRINO-NUCLEON AND ANTINEUTRINO-NUCLEON TOTAL CROSS SECTIONS

T. EICHTEN, H. FAISSNER, F.J. HASERT, S. KABE, W. KRENZ, J. Von KROGH, J. MORFIN and K. SCHULTZE
*III Physikalisches Institut der Technischen Hochschule, Aachen, Germany*

G.H. BERTRAND-COREMANS, J. SACTON, W. Van DONINCK and P. VILAIN*[1]
*Interuniversity Institute for High Energies, U L B , V U B , Brussels, Belgium*

D.C. CUNDY, D. HAIDT, M. JAFFRE, S. NATALI*[2], P. MUSSET, J.B.M. PATTISON, D.H. PERKINS*[3], A. PULLIA, A. ROUSSET, W. VENUS*[4] and H. WACHSMUTH
*CERN, Geneva, Switzerland*

V. BRISSON, B. DEGRANGE, M. HAGUENAUER, L. KLUBERG, U. NGUYEN-KHAC and P. PETIAU
*Laboratoire de Physique Nucléaire des Hautes Energies, Ecole Polytechnique, Paris, France*

E. BELLOTTI, S. BONETTI, D. CAVALLI, C. CONTA*[5], E. FIORINI, C. FRANZINETTI*[6] and M. ROLLIER
*Istituto di Fisica dell'Università, Milano and I.N F.N., Milano, Italy*

B. AUBERT, L.M. CHOUNET, P. HEUSSE, L. JAUNEAU, A.M. LUTZ, C. PASCAUD and J.P. VIALLE
*Laboratoire de l'Accélérateur Linéaire, Orsay, France*

F.W. BULLOCK, M. DERRICK*[7], M.J. ESTEN, T.W. JONES, J. McKENZIE, A.G. MICHETTE*[8], G. MYATT*[3] and W.G. SCOTT*[3,8]
*University College, London, England*

Received 10 August 1973

The $\nu$ and $\bar{\nu}$ nucleon total cross-sections have been determined as a function of energy using a sample of 2500 $\nu$ and 950 $\bar{\nu}$ event. The results are compared with predictions of scaling and charge symmetry hypotheses

Measurements of the total cross-sections for the two processes

$$\nu_\mu + \text{nucleon} \rightarrow \mu^- + \text{hadrons} \quad (1)$$

$$\bar{\nu}_\mu + \text{nucleon} \rightarrow \mu^+ + \text{hadrons} \quad (2)$$

*[1] Chercheur agréé de l'Institut Interuniversitaire des Sciences Nucléaires, Belgique.
*[2] Now at the University of Bari.
*[3] Also at the University of Oxford.
*[4] Now at the Rutherford High Energy Laboratory.
*[5] On leave of absence from the University and INFN-Pavia.
*[6] Also at the University of Turin.
*[7] Visiting research fellow on leave from Argonne National Laboratory.
*[8] Supported by the Science Research Council grant.

have been performed using the large heavy liquid bubble chamber Gargamelle exposed to the $\nu$ and $\bar{\nu}$ beams at the CERN PS. Gargamelle is a cylindrical chamber of length 4.8 m and diameter 1.85 m, placed in a magnetic field of 20 kG. The liquid filling was heavy freon $CF_3Br$ with radiation length $X_0 = 11$ cm and interaction length $L_0 = 60$ cm. The analysis has been carried out using 95 000 and 174 000 pictures taken in the $\nu$ and $\bar{\nu}$ beams, respectively. Only those events located within a fiducial volume of 3 $m^3$ contained in the 7 $m^3$ visible volume of Gargamelle have been measured in the present work. This fiducial volume was chosen to provide a mean potential path length of 150 cm for the particles produced in the $\nu(\bar{\nu})$ interac-



Downloaded from https://www.cambridge.org/core. UNIVERSIDAD AUTONOMA METROPOLITANA, on 17 Nov 2026 at 09:09:05, subject to the Cambridge Core terms of use, available at https://www.cambridge.org/core/terms. https://doi.org/10.1017/9780511609923.010

tions, allowing a reliable separation of the muons from the strongly interacting particles.

Muonic neutrino (antineutrino) induced reactions were characterised by the presence of a negative (positive) muon among the secondary products. Therefore, events containing at least one particle of negative (positive[‡]) charge which did not undergo a strong interaction within the visible volume (absorption, nuclear interaction and/or large angle scattering $> 30°$, or transverse momentum $> 100$ MeV/$c$) were classified as neutrino (antineutrino) events. Of course, there exists a class of ambiguous events (hereafter called $\nu\bar{\nu}$ events) containing at least one "non-interacting" particle of each charge. Events without a muon-signature are called hadronic events [1] and are not analysed further in this paper

The energy of the neutrino (antineutrino) producing a given event was taken to be the total energy liberated in the interaction. The energy taken off by all charged and neutral secondaries must therefore be estimated. The momenta of charged particles were determined from track curvature or range measurements. The energy imparted to the neutrons and $\pi^0$ mesons was obtained by measuring the energy deposited by these particles in the visible volume of the chamber.

The muon energy is measured on average with a precision of about 8%, whilst the charged hadron energy is determined within 15%. Due to the short radiation length of heavy freon, $\gamma$-ray energies are only measured to a precision of about 30%.

Undetected neutrons constitute the main cause of missing energy. Only 75% of the emitted neutrons interact in the visible volume and produce a measurable neutron star. As on average only one third of the energy of a given neutron is deposited in the form of visible energy[‡‡], the neutron energy was obtained by multiplying the visible energy of the neutron star by a factor of 3. Taking these facts into account the energy loss due to undetected neutrons was corrected for empirically by calculating the mean energy taken off by neutrons interactions with associated neutron stars, as a function of the total visible energy ($E$). The mean loss of energy per event was found to be:

for neutrinos $0.045 + 0.015\,E$ GeV

for antineutrinos $0.079 + 0.030\,E$ GeV.

A correction for undetected and unmeasurable $\gamma$-rays was also applied. On average, the energy imparted to an electron-positron pair was found to be 230 MeV, independent of the visible energy liberated in the neutrino interaction. This amount of energy was thus added to the events with an odd number of electron-positron pairs.

Some 7% of the tracks due to hadrons were unmeasurable because the particle interacts after a very short flight path so that any curvature measurement was meaningless. In these cases, either the hadron energy was estimated from an analysis of the secondary star, or if this was impossible, the particle was assigned an energy equal to the mean energy taken off by a hadron, i.e. 500 MeV.

Fast interacting protons and positive pions (kinetic energy $\gtrsim 1$ GeV) cannot be separated by a momentum-ionization analysis. However, as a result of a study of the distribution of $\delta$-rays along their tracks, and the proton range spectrum, more than 80% of these interacting particles were found to be protons. Therefore, in the present study all these particles have been taken as protons.

The average energy correction per event due to all these causes amounts to $\sim (5 \pm 2.5)$% of the visible energy. Having applied these corrections, different cuts were imposed to select the final sample of events.

In order to reduce the background due to charged incoming particles interacting in the fiducial volume, cuts on the longitudinal momentum along the $\nu$ beam axis, $P_L$, and the total energy, $E$, and the four-momentum transfer $q^2$ were applied. Only those events with $P_L > 0.6$ GeV/$c$ and $E \geqslant 1$ GeV and $q^2 \leqslant q^2_{max}$[*] were retained for further analysis.

Events have been discarded when the measurement error was greater than 30%. As a consequence, 4% of the events were rejected, the rejection rate being nearly independent of the value of the total energy

Details of the selected events in both the $\nu$ and $\bar{\nu}$ films are displayed in tables 1 and 2, respectively. The contamination of hadronic events among the $\nu$, $\bar{\nu}$ and $\nu\bar{\nu}$ events has been estimated by calculating the prob-

‡ Stopping protons are easily identified at the scan table.

‡‡ This conclusion is obtained from the examination of all nucleon-nucleon data above 0.5 GeV/$c$

* $q^2_{max}$ is the maximum allowed four-momentum transfer in a neutrino-nucleon collision: $q^2_{max} = 4E^2/(1+2E/M)$ where $M$ is the nucleon mass



Downloaded from https://www.cambridge.org/core. UNIVERSIDAD AUTONOMA METROPOLITANA, on 17 Nov 2026 at 09:09:05, subject to the Cambridge Core terms of use, available at https://www.cambridge.org/core/terms. https://doi.org/10.1017/9780511609923.010

Table 1
Neutrino

| $E$(GeV) | 1–2 | 2–3 | 3–4 | 4–5 | 5–6 | 6–7 | 7–8 | 8–9 | 9–10 | 10 |
|---|---|---|---|---|---|---|---|---|---|---|
| $\nu$ events | 723 | 599 | 324 | 115 | 74 | 40 | 32 | 20 | 26 | 9 |
| $\nu\bar{\nu}$ events | 134 | 197 | 90 | 64 | 27 | 21 | 11 | 9 | 14 | 5 |
| $\bar{\nu}$ events | 44 | 24 | 10 | 9 | 2 | 3 | – | 1 | 1 | 1 |
| Hadronic events | 78 | 34 | 13 | 7 | 5 | – | – | – | – | – |
| Estimated hadronic contamination in $\nu$ events | 14.6 | 5 3 | 2.3 | – | – | 1 2 | – | – | – | – |
| Final total of $\nu$ events | 842 | 791 | 411 | 179 | 101 | 60 | 43 | 29 | 40 | 14 |

Table 2
Antineutrino

| $E$(GeV) | 1–2 | 2–3 | 3–4 | 4–5 | 5–6 | 6–7 | 7–8 | 8–9 | 9–10 | 10 |
|---|---|---|---|---|---|---|---|---|---|---|
| $\bar{\nu}$ events | 313 | 280 | 130 | 69 | 27 | 12 | 6 | 0 | 2 | 1 |
| $\nu$ events | 34 | 24 | 17 | 4 | 6 | – | 1 | – | – | – |
| $\bar{\nu}\nu$ events | 42 | 48 | 28 | 12 | 8 | 4 | 4 | 3 | – | – |
| Estimated $\nu$ in $\bar{\nu}\nu$ events | 5.8 | 8.7 | 4.1 | 2 | 1.9 | – | 0.24 | – | – | – |
| Hadronic events | 44 | 12 | 5 | 1 | 1 | – | – | – | – | – |
| Estimated hadronic contamination in $\bar{\nu}$ events | 13 | 5.5 | 0.3 | 1.5 | – | – | – | – | – | – |
| Final total of $\bar{\nu}$ events | 336 | 314 | 154 | 78 | 33 | 16 | 10 | 3 | 2 | 1 |

ability that a hadronic event can be assigned to any of these three categories. For neutrino events with $E < 2$ GeV, this contamination is found to be of the order of 2%; at higher energy, it becomes negligible.

Since in the $\nu$ beam the $\bar{\nu}$ flux is knwon to be small ($\sim$ 1%), all the $\nu\bar{\nu}$ events observed in the $\nu$ film have been considered as $\nu$ events. In fact all the so-called $\bar{\nu}$ events observed in the $\nu$ film are due to hadronic events in which one, or more positive hadrons leave the chamber without interacting. In the $\bar{\nu}$ film the number of $\nu$ events among the $\nu\bar{\nu}$ sample has been computed using the probability for a $\nu$ event to be ambiguous, as determined from the $\nu$ film.

The neutrino flux and energy spectrum were determined by measuring the muon radial flux distributions at different depths in the steel shielding [2]. The method was improved over the previous CERN neutrino experiments in that the muon flux was monitored continuously Furthermore the K to $\pi$ production ratio has been measured extensively for 24 GeV protons incident on a Be target [2], i.e. at an energy near the one of the protons used in the present experiment (26 GeV).

The estimated error in the $\nu(\bar{\nu})$ spectra, 9% for energies ranging 2 to 6 GeV, is mainly due to the instabilities of the muon flux detectors, varying beam conditions and extrapolation from 24 to 26 GeV of the production data. Above 6 GeV, the error increases to approximately 12% due to uncertainties in the difference of the $\pi$ and K meson absorption in the target. Below 2 GeV, as the neutrinos mainly come from pions for which the production data are not available and the corresponding muon flux cannot be measured, the neutrino flux can only be estimated by extrapolation.

It should be noted that the ratio of the $\nu$ and $\bar{\nu}$ spectra between 2 and 6 GeV is known to an accuracy of about 4%.

The total cross sections for $\nu$ and $\bar{\nu}$ are shown in fig. 1. The cross-sections for the quasi-elastic processes:

$$\nu_\mu + n \rightarrow \mu^- + p, \qquad \bar{\nu}_\mu + p \rightarrow \mu^+ + n$$



Downloaded from https://www.cambridge.org/core. UNIVERSIDAD AUTONOMA METROPOLITANA, on 17 Nov 2026 at 09:09:05, subject to the Cambridge Core terms of use, available at https://www.cambridge.org/core/terms. https://doi.org/10.1017/9780511609923.010

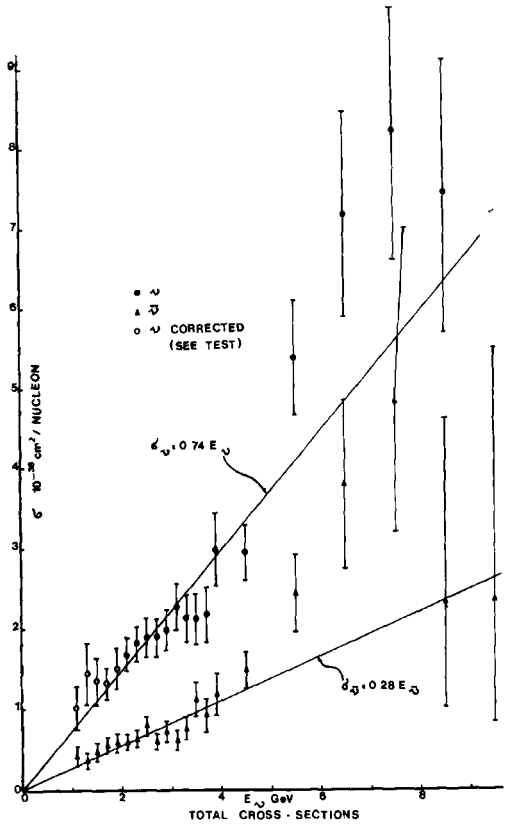



Fig. 1. Total neutrino and antineutrino cross-sections as a function of energy.

have also been determined, and are shown in fig. 2. For this analysis an elastic $\nu$ event is defined as one containing a single $\mu^-$ accompanied by not more than one proton of kinetic energy $> 30$ MeV.

An elastic antineutrino event is defined as one containing a single $\mu^+$, no proton $> 30$ MeV and not more than one neutron $> 30$ MeV. A special scan assured that the scanning efficiency for this type of event was $\sim 100\%$.

As stated above the flux between 1–2 GeV is not known with precision. Above 2 GeV the measured value of both the $\nu$ and $\bar\nu$ cross-sections are compatible with those expected using electromagnetic nucleon form-factors.

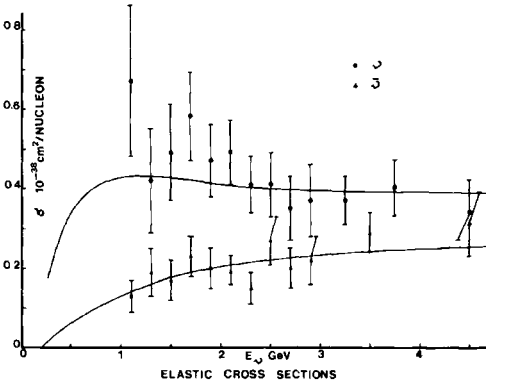



Fig. 2. Elastic neutrino and antineutrino cross-sections as a function of energy.

The curves shown in fig. 2 are the best fits for the elastic cross-section corrected for nuclear effects [3] for energies above 2 GeV.

From discrepancy of the neutrino elastic cross-section observed below 2 GeV, it is concluded that the extrapolation of the $\nu$ flux in this region is incorrect. Therefore the total cross-section measurements below 2 GeV have been corrected using the observed difference between the measured and expected elastic $\nu$ cross-section.

For the total $\nu$ and $\bar\nu$ cross-section data in fig. 1, best straight-lines have been fitted. In this fit account has been taken of the distortion expected for a linearly rising $\nu$, $\bar\nu$ cross section due to very rapidly falling $\nu$, $\bar\nu$ spectra and the measurement errors. The correction is of the order of ± 3%, except at 6 GeV where the cross-section is over-estimated by 10%. The best linear fits to the cross-sections are shown in table 3.

Table 3

| | | one parameter fit | two parameter fit |
|---|---|---|---|
| $E > 1$ GeV | $\nu$ | $(0.74\pm0.02)E$ | $(0.70\pm0.07)E + (0.14\pm0.18)$ |
| | $\bar\nu$ | $(0.28\pm0.01)E$ | $(0.26\pm0.04)E + (0.05\pm0.09)$ |
| $E > 2$ GeV | $\nu$ | $(0.74\pm0.03)E$ | $(0.77\pm0.09)E - (0.11\pm0.25)$ |
| | $\bar\nu$ | $(0.27\pm0.01)E$ | $(0.32\pm0.06)E - (0.13\pm0.17)$ |



Downloaded from https://www.cambridge.org/core. UNIVERSIDAD AUTONOMA METROPOLITANA, on 17 Nov 2026 at 09:09:05, subject to the Cambridge Core terms of use, available at https://www.cambridge.org/core/terms. https://doi.org/10.1017/9780511609923.010

Volume 46B, number 2 PHYSICS LETTERS 17 September 1973

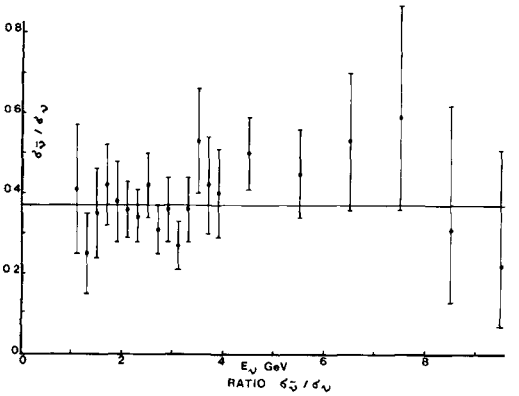



Fig. 3 The ratio $R = \sigma(\bar\nu)/\sigma(\nu)$ of antineutrino to neutrino cross-sections as a function of energy.

To the extent that the $\nu$ and $\bar\nu$ cross-sections rise in an approximately linear fashion with energy, the data are consistent with the scaling hypothesis [4] which is well verified in the SLAC deep inelastic electron-nucleon scattering experiments [5].

Fig. 3 shows the ratio $R_1 = \sigma(\bar\nu)/\sigma(\nu)$ of antineutrino to neutrino cross-sections as a function of energy $E$. Within the errors, $R_1$, is compatible with a constant independent of energy. The average are:

$R_1 = 0.37 \pm 0.02, \quad E > 1$ GeV,

$R_1 = 0.38 \pm 0.02, \quad E > 2$ GeV.

Scaling also implies a linear energy dependence of the mean value of $q^2$, called $\langle q^2 \rangle$. Fig. 4 shows the mean value $\langle q^2 \rangle$. Fig. 4 shows the mean value $\langle q^2 \rangle$ plotted against neutrino energy $E$, for events in the $\nu$ and $\bar\nu$ film. The results of linear fits are:

neutrino $\langle q^2 \rangle = 0.12 \pm 0.03 + (0.23 \pm 0.01)E$

antineutrino $\langle q^2 \rangle = 0.09 \pm 0.03 + (0.14 \pm 0.015)E$ $\quad E > 1$ GeV

neutrino $\langle q^2 \rangle = (0.22 \pm 0.06) + (0.21 \pm 0.02)E$

antineutrino $\langle q^2 \rangle = (0.11 \pm 0.08) + (0.14 \pm 0.03)E$ $\quad E > 2$ GeV.

The error on the slope depends very little on possible systematic errors in measuring the hadron energy in the events. For example, at $E = 4$ GeV, an 8% error in $E$ results only in a 2% error in $q^2$ and therefore in the slope of the line.

The analysis of the energy transfer distributions ($y$) will be discussed in a forthcoming paper because it involves weighting procedures to take account of the $\pi, \mu$ ambiguities

The foregoing results are now discussed in terms of the hypotheses of scale invariance and charge symmetry However it should first be emphasized that most of the events have rather low energy, and are not in the "deep-inelastic" region, where $q^2 \gg M^2$ and $\nu \gg M$ ($\nu$ is the energy transfer, $E - E_\mu$), which are the conditions for scaling, as observed in the SLAC electron scattering experiments.

The scaling region cross-sections have the form:

$$\frac{d^2\sigma^{\nu,\bar\nu}}{dx\,dy} = \frac{G^2 ME}{\pi}\left[(1-y)F_2(x) + \frac{y^2}{2}\left[2xF_1(x)\right] \mp y\left(1-\frac{y}{2}\right)xF_3(x)\right],$$

where $x = q^2/2M\nu$ and $y = \nu/E$ are dimensionless variables. For an equal number of neutron and proton targets, as is approximately true in the heavy liquid employed in the experiment, the hypothesis of charge symmetry of $\Delta S = 0$ weak processes results in the same values of the structure functions $F_i$ for neutrinos and antineutrinos.

Experimentally, the cross-section ratio $R_1$ is close to the lowest bound allowed by scaling and charge symmetry i.e. 1/3. For this reason it is possible to obtain stringent bounds for ratios of the structure functions. In the case of $A = \int 2xF_1(x)\,dx / \int F_2(x)\,dx$ the bounds are:

$$(0.87 \pm 0.05) = \frac{3 - 3R_1}{1 + 3R_1} \leqslant A \leqslant 1.$$

This is in agreement with the Callan-Gross relation [6] as well as with the value found in the SLAC electroproduction experiments [5]. In terms of the parton model, a ratio equal to unity would imply partons of spin 1/2 only.

A similar bound can be obtained for the interference term, denoted by $B = -\int xF_3(x)\,dx / \int F_2(x)\,dx$, of·

$$(0.90 \pm 0\,04) = \frac{2(3-3R_1)}{3+3R_1} \geqslant B \geqslant \frac{(3-3R_1)}{1+3R_1} = (0.87 \pm 0.05).$$



Downloaded from https://www.cambridge.org/core. UNIVERSIDAD AUTONOMA METROPOLITANA, on 17 Nov 2026 at 09:09:05, subject to the Cambridge Core terms of use, available at https://www.cambridge.org/core/terms. https://doi.org/10.1017/9780511609923.010

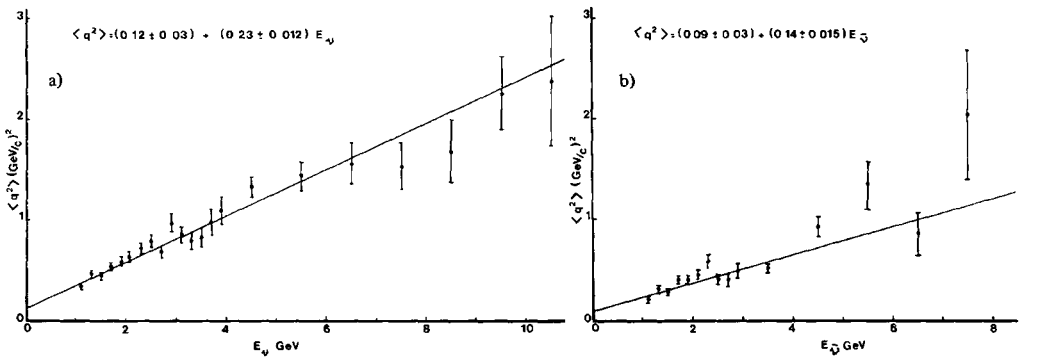



Fig. 4. (a) The mean value $\langle q^2 \rangle$ versus energy for neutrino interactions. (b) The mean value $\langle q^2 \rangle$ versus energy for antineutrino interactions.

The left limit is valid if one assumes the integrated Callan-Gross relation, i.e. $A = 1$. The fact that $B$ is close to unity implies that parity is violated almost maximally.

Without making any additional assumptions scaling and charge symmetry can be tested by considering the average values $\langle xy \rangle_\nu$ and $\langle xy \rangle_{\bar{\nu}}$. The positivity conditions for the absorption of left, righthanded or scalar currents by the nucleon imply the following inequalities [7]:

$$5(1+R_1) \geqslant 16(\langle xy \rangle_\nu - R_1 \langle xy \rangle_{\bar{\nu}})$$

$$7(1+R_1) \geqslant 16(\langle xy \rangle_\nu + R_1 \langle xy \rangle_{\bar{\nu}})$$

$$36 \langle xy \rangle_\nu \geqslant 6 R_1 \langle xy \rangle_{\bar{\nu}} \geqslant \langle xy \rangle_\nu$$

$$35(3R_1 - 1) + 32 \langle xy \rangle_\nu \geqslant 192 R_1 \langle xy \rangle_{\bar{\nu}}.$$

As $\langle q^2/E \rangle = 2M \langle xy \rangle$, the $\langle q^2 \rangle$ versus $E$ plots give:

$$\langle xy \rangle_\nu = 0.12 \pm 0.01$$

$$\langle xy \rangle_{\bar{\nu}} = 0.07 \pm 0.01.$$

Hence, as the four above inequalities are satisfied by these experimental values, there is no indication of a violation of charge symmetry.

In addition assuming the local Callan-Gross relation $2xF_1(x) = F_2(x)$ it can be shown that

$$R_2 \equiv \frac{\langle xy \rangle_{\bar{\nu}}}{\langle xy \rangle_\nu} = \frac{7 - 5B'}{R_1(7 + 5B')}$$

where

$$B' = -\int x(xF_3(x))\,dx \Big/ \int xF_2(x)\,dx.$$

Experimentally

$$B' = 0.87 \pm 0.08.$$

The ratios $B$ and $B'$ are expected to be equal if $(xF_3(x))$ and $F_2(x)$ have the same functional $x$-dependence. The fact that $B$ and $B'$ are equal within the errors is compatible with this.

The value for the integral $\int F_2(x)\,dx$ can be determined from the relation:

$$\sigma^\nu - \sigma^{\bar{\nu}} = \frac{G^2 ME}{\pi} \int F_2(x)\,dx\,(\tfrac{2}{3} B),$$

to be

$$0.49 \pm 0.03 \leqslant \int F_2(x)\,dx \leqslant 0.51 \pm 0.03.$$

In the parton model this integral is interpreted as the relative momentum carried by isovector partons

$$\int F_2(x)\,dx = \int x(U + D + \bar{U} + \bar{D})\,dx,$$

where $U$, $D$, $\bar{U}$, $\bar{D}$ are the isospin "up" and isospin "down" parton and antiparton momentum distribution functions in the proton. Therefore approximately 50% of the nucleon momentum is carried by either isoscalar partons or gluons.

The contribution of antipartons (isovector) can be estimated by means of the following relation [8]

$$\frac{\int x(\bar{U} + \bar{D})\,dx}{\int x(U + D)\,dx} \leqslant \tfrac{3}{8}(3R_1 - 1) = 0.05 \pm 0.02.$$



Downloaded from https://www.cambridge.org/core. UNIVERSIDAD AUTONOMA METROPOLITANA, on 17 Nov 2026 at 09:09:05, subject to the Cambridge Core terms of use, available at https://www.cambridge.org/core/terms. https://doi.org/10.1017/9780511609923.010

Volume 46B, number 2 PHYSICS LETETRS 17 September 1973

## References

[1] F J. Hasert et al., Phys Lett. 46B (1973) 138.
[2] D. Bloess et al., Nuclear Instr. Methods 91 (1971) 605.
[3] J Lǿvseth, Nuovo Cim. 57A (1968) 382.
[4] J D Bjorken, Phys. Rev. 179 (1969) 1547.
[5] G Miller et al., Phys. Rev. D5 (1972) 528;
E D Bloom et al., Phys. Rev. Lett. 23 (1969) 930
[6] C.G Callan and D.G. Gross, Phys. Rev Lett. 22 (1969) 156.
[7] A. de Rujula and S L Glashow, Harvard Preprint (May 1973).
[8] E.A. Paschos, NAL Preprint-NAL Conf ,- 73/27 - THY (April 1973)



Downloaded from https://www.cambridge.org/core. UNIVERSIDAD AUTONOMA METROPOLITANA, on 17 Nov 2026 at 09:09:05, subject to the Cambridge Core terms of use, available at https://www.cambridge.org/core/terms. https://doi.org/10.1017/9780511609923.010